Neurobiology of Disease

Neuronopathic GBA1L444P Mutation Accelerates Glucosylsphingosine Levels and Formation of Hippocampal Alpha-Synuclein Inclusions

Casey L. Mahoney-Crane,[1*] Megha Viswanathan,[1*] Dreson Russell,[1] Rachel A.C. Curtiss,[1] Jennifer Freire,[1] Sai Sumedha Bobba,[1] Sean D. Coyle,[1] Monika Kandebo,[2] Lihang Yao,[2] Bang-Lin Wan,[2] Nathan G. Hatcher,[2] Sean M. Smith,[2] Jacob N. Marcus,[2] and Laura A. Volpicelli-Daley[1]

[1]Center for Neurodegeneration and Experimental Therapeutics, University of Alabama at Birmingham, Birmingham, Alabama 35294 and [2]Neuroscience Discovery, Merck & Company, Inc, West Point, Pennsylvania 19486

The most common genetic risk factor for Parkinson's disease (PD) is heterozygous mutations *GBA1*, which encodes for the lysosomal enzyme, glucocerebrosidase. Reduced glucocerebrosidase activity associates with an accumulation of abnormal α-synuclein (α-syn) called Lewy pathology, which characterizes PD. PD patients heterozygous for the neuronotypic GBA1L444P mutation ($GBA1^{+/L444P}$) have a 5.6-fold increased risk of cognitive impairments. In this study, we used $GBA1^{+/L444P}$ mice of either sex to determine its effects on lipid metabolism, expression of synaptic proteins, behavior, and α-syn inclusion formation. At 3 months of age, $GBA1^{+/L444P}$ mice demonstrated impaired contextual fear conditioning, and increased motor activity. Hippocampal levels of vGLUT1 were selectively reduced in $GBA1^{+/L444P}$ mice. We show, using mass spectrometry, that GBA1L444P expression increased levels of glucosylsphingosine, but not glucosylceramide, in the brains and serum of $GBA1^{+/L444P}$ mice. Templated induction of α-syn pathology in mice showed an increase in α-syn inclusion formation in the hippocampus of $GBA1^{+/L444P}$ mice compared with $GBA1^{+/+}$ mice, but not in the cortex, or substantia nigra pars compacta. Pathologic α-syn reduced SNc dopamine neurons by 50% in both $GBA1^{+/+}$ and $GBA1^{+/L444P}$ mice. Treatment with a GlcCer synthase inhibitor did not affect abundance of α-syn inclusions in the hippocampus or rescue dopamine neuron loss. Overall, these data suggest the importance of evaluating the contribution of elevated glucosylsphingosine to PD phenotypes. Further, our data suggest that expression of neuronotypic GBA1L444P may cause defects in the hippocampus, which may be a mechanism by which cognitive decline is more prevalent in individuals with GBA1-PD.

Key words: α-synuclein; glucocerebrosidase; glucosylceramide; glucosylsphingosine; Parkinson's disease; venglustat

Significance Statement

Parkinson's disease (PD) and dementia with Lewy bodies (*DLB*) are both pathologically characterized by abnormal α-synuclein (α-syn). Mutant *GBA1* is a risk factor for both PD and DLB. Our data show the expression of neuronotypic GBA1L444P impairs behaviors related to hippocampal function, reduces expression of a hippocampal excitatory synaptic protein, and that the hippocampus is more susceptible to α-syn inclusion formation. Further, our data strengthen support for the importance of evaluating the contribution of glucosylsphingosine to PD phenotypes. These outcomes suggest potential mechanisms by which GBA1L444P contributes to the cognitive symptoms clinically observed in PD and DLB. Our findings also highlight the importance of glucosylsphingosine as a relevant biomarker for future therapeutics.

Received Mar. 25, 2022; revised Sep. 9, 2022; accepted Nov. 10, 2022.

Author contributions: C.L.M.-C., M.V., S.M.S., J.N.M., and L.A.V.-D. designed research; C.L.M.-C., M.V., D.R., R.A.C.C., J.F., S.B., S.D.C., M.K., L.Y., B.-L.W., and N.G.H. performed research; C.L.M.-C., M.V., D.R., R.A.C.C., J.F., S.B., S.D.C., M.K., L.Y., N.G.H., and J.N.M. analyzed data; C.L.M.-C. wrote the first draft of the paper; C.L.M.-C., M.V., D.R., R.A.C.C., J.F., S.B., S.D.C., N.G.H., S.M.S., J.N.M., and L.A.V.-D. edited the paper; C.L.M.-C., M.V., D.R., and L.A.V.-D. wrote the paper.

This work was supported by National Institutes of Health (NIH) National Institute of Neurological Disorders and Stroke (NINDS) Grant R01 NS102257 to L.A.V.-D.; NIH NINDS Grant R56 NS117465 to L.A.V.-D.; NIH NINDS Grant T32 NS095775 to C.L.M.-C.; Parkinson Foundation P13 postdoctoral fellowship to R.A.C.C.; and Parkinson's Association of Alabama. All behavioral experiments were performed in the UAB Behavioral Assessment Core A. We thank Valentina Krendelchtchikova for her help with purifying recombinant α-synuclein; Nicholas Boyle for help with protocols; Dr. Karen Gamble and Dr. Richard Kennedy for advice on statistics; and Dr. Joseph Mazzulli for the suggestion to characterize the GBA1L444P mice without fibrils or injections.

*C.L.M.-C. and M.V. contributed equally to this work.

M.K., L.Y., B.-L.W., N.G.H., S.M.S., and J.N.M. are shareholders of Merck. Remaining authors declare no competing financial interests.

Correspondence should be addressed to Laura A. Volpicelli-Daley at lvolpicellidaley@uabmc.edu.

https://doi.org/10.1523/JNEUROSCI.0680-22.2022

Introduction

Synucleinopathies, such as Parkinson's disease (PD) and Lewy body dementias, are characterized by the neuronal accumulation of α-synuclein (α-syn) aggregates which are phosphorylated (p-α-syn), called Lewy pathology. Historically, most research has focused on the role of Lewy pathology in the death of dopamine neurons because of the contribution to motor symptoms of PD. However, Lewy pathology is significantly correlated with increased PD dementia (PDD) (Irwin et al., 2012). PD patients with the severe L444P mutation in the *GBA1* gene show up to a 5.6-fold increase in the risk for dementia (Cilia et al., 2016). The severity of the GBA1L444P mutation can be classified based on the location of the mutation contributing to unstable glucocerebrosidase (GCase) because of a conformational change as well as showing a correlation in increased cognitive decline severity (Dvir et al., 2003; Migdalska-Richards and Schapira, 2016; Szwedo et al., 2022; Vieira and Schapira, 2022). In addition, the GBA1L444P heterozygous mutation is one of the most prevalent mutations in PD. Nearly 8%-12% of PD cases occur because of a mutation in *GBA1* (GBA1-PD), which is the most common risk factor for PD, after aging (Stoker and Greenland, 2018). The severe $GBA1^{+/L444P}$ mutation represents ~35% of all *GBA1* mutations linked to PD (Sidransky et al., 2009). Thus, the interaction between mutant *GBA1* and the formation of Lewy pathology may contribute to cognitive decline in PD.

GBA1 encodes for the lysosomal enzyme, GCase, which metabolizes the sphingolipids glucosylceramide (GlcCer) to glucose and ceramide (Do et al., 2019; Boer et al., 2020). The GBA1L444P mutation impairs proper folding of the enzyme, preventing its transport from the endoplasmic reticulum to the Golgi apparatus and lysosomes. Previous studies evaluating mice heterozygous for GBA1L444P revealed a reduction of GCase activity by ~40% (Fishbein et al., 2014). Mouse models of α-synucleinopathies show that mice heterozygous for GBA1L444P have increased pathologic α-syn aggregate formation and motor defects (Taguchi et al., 2017; Migdalska-Richards et al., 2020), suggesting that reduced GCase activity promotes accumulation of Lewy pathology.

Here, we show reduced GCase activity in the cortex, striatum, hippocampus, and midbrain of $GBA1^{+/L444P}$ knock-in mice relative to wildtype ($GBA1^{+/+}$) mice. $GBA1^{+/L444P}$ mice and aged $GBA1^{+/+}$ mice show increased brain levels of glucosylsphingosine (GlcSph), but not GlcCer which is consistent with previous findings (Taguchi et al., 2016; Polinski et al., 2021). $GBA1^{+/L444P}$ mice also show reduced levels of the presynaptic protein, vGLUT1, and impairments in contextual fear conditioning, suggesting that mutant GBA1 alone causes neuronal defects in limbic brain regions. $GBA1^{+/L444P}$ mice also show increased motor activity. To determine the impact of $GBA1^{+/L444P}$ on the formation of α-syn aggregates and neuronal toxicity, mice were analyzed after injections of α-syn preformed fibrils (PFFs) to induce corruption of endogenously expressed α-syn. There was increased α-syn pathology in the hippocampus of $GBA1^{+/L444P}$ knock-in mice compared with $GBA1^{+/+}$ mice, but this did not occur in the SNc or cortex. Expression of $GBA1^{+/L444P}$ did not enhance α-syn inclusion-induced loss of dopamine neurons in the SNc compared with $GBA1^{+/+}$ mice. Treatments with a GlcCer synthase (GCS) inhibitor did not prevent α-syn inclusion formation in primary cultured neurons or in fibril-injected mice. Overall, these data suggest that expression of GBA1L444P increases the susceptibility of hippocampal neurons to dysfunction and the formation of α-syn inclusions in the hippocampus. These findings also support GlcSph is a potential target for therapeutics and plasma GlcSph as a putative biomarker for GBA1-PD.

Materials and Methods

Animal care

All animal protocols were approved by the University of Alabama at Birmingham's Institutional Animal Care and Use Committee. Both male and female *GBA1* mice heterozygous for the L444P mutation ($GBA1^{+/L444P}$), obtained from the Mutant Mouse Resource and Research Center (MMRRC-000117) at the University of North Carolina at Chapel Hill, were used for these studies and generated as previously described (Liu et al., 1998). Mice were on a 12 h light/dark cycle and had ad libitum access to food and water.

Fibril preparation

Fibrils were prepared as previously described (Stoyka et al., 2020, 2021). Mouse monomeric α-syn was purified from *Escherichia coli*, and endotoxin was removed using the Pierce high-capacity endotoxin spin columns and quantified using the Pierce endotoxin chromogenic quantification kit (Volpicelli-Daley et al., 2014; Stoyka et al., 2021). Monomeric α-syn was stored at concentrations >10 mg/ml at −80°C. To generate fibrils, monomer was rapidly thawed and centrifuged at 20,000 × *g*. The concentration of the supernatant was determined using A280 nm with an extinction coefficient of 7450 $M^{-1}\,cm^{-1}$ using a NanoDrop 2000/2000c Spectrophotometer (Fisher Scientific catalog #ND-2000) and diluted to 5 mg/ml in 150 mM KCl and 50 mM Tris-HCl. A volume of 500 μl was shaken at 37°C at 700 rpm for 7 d. The fibrils were spun for 10 min at 16,363 *g* at room temperature and resuspended in 250 μl of the above buffer. To determine the concentration of PFFs, 5 μl was incubated with 5 μl of 8 M guanidinium chloride to dissociate the fibrils, and the concentration was measured using A280 nm. Buffer was added to the fibrils to obtain a final concentration of 5 mg/ml, aliquoted to 25 μl, and stored at −80°C until use. On the day of injection, fibrils were sonicated using a QSonica700 cup horn sonicator with a 16°C water bath for 15 min at 30% amplitude for 3 s on and 2 s off pulse at 85,824 joules. Fragmentation of fibrils was confirmed using dynamic light scattering.

Bilateral striatal injection of fibrils

Three-month-old mice were anesthetized with vaporized isoflurane (1%) on a stereotactic setup (Kopf, model 940, small animal stereotaxic instrument, standard accessories). The scalp was shaved and wiped with chlorhexidine, and a vertical incision was made. Bilateral coordinates relative to bregma were 1 mm anterior, ±2.0 mm lateral, and −3.2 mm ventral relative to the skull. Two microliters of sonicated fibrils (5 μg/μl) or monomeric α-syn (5 μg/μl) was injected at a constant rate of 0.5 μl/min. The needle was left in place for 4 min to allow diffusion, then retracted 1 mm, then left in place for another 1 min before fully retracting the needle. Scalp incisions were closed with EZ-Clips. Mice were administered 10 units of 1.5 mg/ml carprofen subcutaneously the next day.

Starting 1 week after injections, mice were fed chow containing venglustat or control chow without venglustat (Research Diets) provided by Merck. Venglustat was used as eliglustat cannot cross the blood–brain barrier efficiently. Male and female mice were fed separate chow formulations with the concentration of venglustat targeting a dose of 60 mg venglustat/kg body weight/day based on the mean expected food consumption and the mean body weight of male and female mice. Cages were allocated 5 g chow per mouse, and food was replenished every week, or as needed. Mice were kept on the formulated chow until the day of death.

Behavior testing

Behavior testing was performed as previously described at the UAB McKnight Behavior Core (Stoyka et al., 2020, 2021). Mice were acclimated for 30 min under a white sheet until the time of the test. Each test was run with operator silence and, when available, the assistance of a white noise machine to minimize potentially intrusive noises. The operator was blinded to treatment and genotype. Tests were performed in the

following order: pole test, open field test, and fear conditioning (contextual then cued).

Open field. Open field test was run on each mouse using ActivityMDB program to track motion in a 1 × 1 foot enclosed field with two zones of detection: Zone 0 and Zone 1. Zone 1 was defined as the center of the box, whereas Zone 0 was the perimeter of the box. This tracking monitored the velocity of movement, and time spent in each zone over the course of 10 min. The percent time in the center was calculated as (the time spent in zone 1 divided by the total time spent in the box) × 100.

Pole test. The pole test was conducted using a 12 inch wooden dowel rod with a diameter of 1.27 cm, anchored with a 4 × 6 × 1 inch block of wood and ridged at 1 inch intervals with rolled rubber bands. The dowel rod was placed vertically in the center of a 1 × 1 foot enclosure. The mice were trained once by being placed face-down at the base of the pole and allowed to climb off onto the floor of the enclosure before being returned to their cage. Following this, each mouse was placed face-up at the top of the pole and allowed no more than 180 s to turn around and climb down to the bottom; this was repeated 5 times. Mice were given a minimum of 30 s to rest between each trial. Three time point measurements were recorded. The first time point started from the time the mouse was placed on the pole to the time taken for the mouse to reach the bottom (total descent time). Measurements were recorded for the time the mouse took to turn around on the pole to face the bottom (turnaround time) and the total time to descend (time descending) in seconds. The average time for each time point was calculated from all five trials for each mouse.

Fear conditioning. Fear conditioning was performed using an apparatus designed with a grid of metal bars on the floor and connected to an electrical output box set to 0.6 mAmp controlled by the VideoFreeze software. On day 1, mice were individually placed in the apparatus; and after 2 min, a 30 s tone was presented with a 2 s mild foot shock at the last 2 s of the tone. The mouse was allowed to rest for 60 s, followed by a second delivery of tone and shock. The mouse was allowed to rest for 60 s after the second mild foot shock. This was completed once per mouse. Freezing was measured manually by a researcher blinded to treatment and genotype. Percent time freezing was calculated as the time (in seconds) the mouse did not move divided by the total time of each time point (e.g., 0-120 s or 120-150 s). The conditioned stimulus (CS) was defined as the tone played, and the unconditioned stimulus (US) is the mild foot shock.

The following day, the mice performed the "Contextual" test. The mice were placed in the fear conditioning apparatus with an identical environment as training. Freeze times of each mouse over the course of 5 min (300 s) were recorded. Percent time freezing was calculated as the time (in seconds) the mouse did not move divided by the total time. The first minute (60 s) was graphed.

On day 3, "Cued" fear conditioning was performed in the same apparatus by replacing the metal bars on the bottom with solid white tiles. Solid white tiles were also placed inside the monitored area, changing the environment from a square cage with metal bars on the floor to a solid white triangular container. The cage was cleaned using 70% Ethanol and treated with a small drop of concentrated peppermint oil to conceal any familiar scents. The area surrounding the cage was changed by placing a purple and white striped pattern along the wall. The same CS used for training was presented for 30 s, without the US, followed by a 60 s rest and repeated twice for a total of 300 s. Freeze times of each mouse were measured over the course of 5 min (300 s). The average percent time the mouse spent freezing during the two tones was graphed.

Immunohistochemistry (IHC) and immunofluorescence (IF)

Ten months after injection, mice were anesthetized with isoflurane and transcardially perfused with saline solution (0.9% NaCl, 0.005% sodium nitroprusside, and 10 units/ml heparin sodium) followed by cold 4% PFA in PBS using gravity perfusion. Brains were removed and postfixed for 24 h in 4% PFA followed by 30% sucrose PBS solution for 48 h. Brains were then frozen in methylbutane solution (−50°C to −60°C) and sectioned into 40 μm serial sections with a freezing microtome (Leica SM 2010R). Serial sections spaced 240 μm apart representing the entire forebrain were collected in a 6-well tray using a freezing microtome (Stoyka et al., 2020, 2021). Sections were stored at −20°C in a solution of 50% glycerol, and 0.01% sodium azide in TBS.

All incubations and rinses were performed using an orbital shaker. For IHC, sections were rinsed 3 times in TBS and quenched in 3% H_2O_2 in TBS for 10 min. Following three rinses in TBS, sections were incubated in antigen retrieval solution (10 mM sodium citrate, 0.05% Tween 20, pH 6) at 37°C for 1 h, rinsed 3 times in TBS, and blocked using 5% normal donkey serum (Equitech-Bio) with 0.1% Triton X-100 in TBS for 1 h at 4°C. After blocking, sections were incubated in primary antibody solution of rabbit polyclonal antibody to TH (Sigma AB152, RRID: AB_390204) in 5% normal donkey serum in TBS at 4°C overnight. After three rinses, sections were then incubated in Biotin-SP AffiniPure Donkey Anti-Rabbit IgG H&L (Jackson ImmunoResearch Laboratories 711-065-152) in 5% normal donkey serum in TBS for 2 h, followed by incubation with Avidin-Biotin Complex Peroxidase Standard Staining kit reagent (ABC; Fisher Scientific) for 1 h at room temperature. Sections were developed using ImmPACT-DAB (Vector Labs), sequentially dehydrated as previously described (Stoyka et al., 2020, 2021) and mounted on charged slides using Permount.

For IF, sections were rinsed 3 times in TBS and incubated in an antigen retrieval solution (10 mM sodium citrate, 0.05% Tween-20, pH 6.0) for 1 h at 37°C. Sections were rinsed 3 times in TBS and blocked and permeabilized in 5% normal goat serum, 0.1% Triton X-100 in TBS for 1 h at 4°C. Sections were rinsed 3 times in TBS and then incubated in a primary antibody solution with 5% normal goat serum in TBS overnight at 4°C. Primary antibodies used included p-α-syn (Abcam, catalog #ab51253, RRID:AB_869973), TH (Abcam, catalog #ab76442, RRID:AB_1524535), and total synuclein (BDTrans, catalog #610786, RRID:AB_398107). Sections were rinsed 3 times in TBS and incubated with secondary antibodies (1:500) in 5% goat serum in TBS overnight at 4°C. Secondary antibodies were AlexaFluor goat anti-rabbit 555 IgG (Fisher Scientific, catalog #A-21429, RRID: AB_2535850), AlexaFluor goat anti-mouse 647 IgG_1 (Fisher Scientific, catalog #A-21240, RRID:AB_2535809), AlexaFluor goat anti-chicken 488 IgY (Fisher Scientific, catalog #A-11039, RRID:AB_2534096), and Hoechst 33342 (1:1000). Sections were rinsed 3 times in TBS and mounted on charged glass slides with Prolong Gold (Invitrogen).

Quantification of p-α-syn inclusions in brain sections

Images and quantitation were performed by a researcher blinded to experimental conditions. Sections were imaged on Nikon C2 confocal microscope at 10× magnification and analyzed using ImageJ software. Images of the basolateral amygdala, hippocampus, SNc, and dorsomedial PFC (dmPFC) were captured from the fibril-injected brains. Representative images were matched across samples to ensure consistency in the relative positions (according to bregma coordinates) of the regions imaged. One image from one of the hemispheres was captured of the dmPFC and one image each from both hemispheres was captured for the other ROIs. Several images were tiled together to create a single, large-field image of the larger regions, the dmPFC, and hippocampus, using the Nikon Elements imaging software.

p-α-syn inclusions were quantified using the CellCounter program on ImageJ. ROIs were drawn manually on ImageJ. For the hippocampal images, separate ROIs (dentate gyrus, CA1, CA3) were drawn demarcating the layers. Images were thresholded using the "maximum threshold" option on Fiji, by setting the same maximum brightness for all images for each region. The threshold was set to 180 for hippocampal and SNc images, 810 for all amygdala images, and 315 for all dmPFC images. For entorhinal cortical images, images were not thresholded. This ensured that all inclusions were clearly visible. Neuritic and somal aggregates were counted manually using the CellCounter program, and each hemisphere was evaluated separately. The average of both hemispheres for each mouse was calculated and graphed.

Unbiased stereology

Unbiased stereology was conducted using the Olympus BX51 bright field microscope and the optical fractionator probe (Stereo Investigator

software, Stereology Resource Center) to analyze TH neurons in the SNc. On average, five or six sections of the SNc from rostral to caudal (spaced 160 µm apart) were quantified. Quantification was conducted with a counting frame of 50 µm × 50 µm, optical dissector height of 22 µm, and section thickness of 33 µm. The measured counting variability for Schmitz-Hof coefficient of error was below 0.135 for all mice.

Primary hippocampal neurons

Embryonic day 16-18 embryos from a GBA1$^{+/L444P}$ cross were removed and hippocampal tissue from each embryo was dissected and placed in individual Falcon tubes containing 10 ml Hibernate E solution. Neurons were cultured as previously described (Volpicelli-Daley et al., 2014), and neurons from each embryo were plated separately in 24-well plates with coverslips. Tails from each embryo were used to determine genotype.

Treating primary hippocampal neurons

On DIV7, fibrils were diluted to 100 µg/ml in PBS and sonicated using a probe-tip sonicator (Fisher Scientific, model CL-18) for 30 s with a 1 s pulse at 30% amplitude. Sonicated fibrils were diluted to 0.1 µg/ml in neuronal media. Neurons were treated with fibrils (0.1 µg/ml) or monomers (0.1 µg/ml). Twenty-four hours after fibril or monomer treatment, neurons were treated with 100 nM Eliglustat (Sigma, SML3212) or equal volume DMSO.

IF of cultured hippocampal neurons

Neurons were fixed in 4% PFA/4% sucrose solution in PBS at room temperature for 30 min. After rinsing 4 times in PBS, neurons were blocked and permeabilized with 3% BSA and 0.05% saponin in PBS for 30 min at room temperature. Neurons were then incubated in primary antibody in 3% BSA and 0.05% saponin overnight at 4°C. The primary antibodies used were neurofilament heavy polypeptide (Abcam, catalog #ab722996, RRID:AB_2119618), p-α-syn (Abcam, catalog #ab51253, RRID:AB_869973), and total α/β-synuclein 202 (BioLegend, catalog #836602, RRID:AB_2734606). Neurons were rinsed 3 times in PBS with 0.05% saponin and incubated in secondary antibody in 3% BSA and 0.05% saponin for 1 h at room temperature. Secondary antibodies used were AlexaFluor goat anti-rabbit 488 IgG (Fisher Scientific, catalog #A-11034, RRID:AB_2576217), AlexaFluor goat anti-mouse 555 IgG_{2a} (Fisher Scientific, catalog #A-21137, RRID:AB_2535776), AlexaFluor goat anti-chicken 647 IgY (Fisher Scientific, catalog #A-21449, RRID:AB_2535866), and Hoechst 33342 (1:1000). Neurons were then rinsed twice in PBS with 0.05% saponin and 3 times with PBS and mounted with Prolong Gold (Invitrogen). Five representative fields per coverslip were imaged using Nikon A1R confocal microscope with a 40× oil-immersion objective. Images were analyzed using ImageJ software by selecting the "IsoData" auto-threshold option. Percent area occupied by fluorescent signal was calculated using "particle analysis" in ImageJ. The percent area of p-α-syn was normalized by dividing by the percent area occupied by neurofilament-H IF.

DQ-BSA red in cultured hippocampal neurons

DQ-BSA Red (Invitrogen) was solubilized in 1 ml PBS to a stock concentration of 1 mg/ml and sonicated with a probe tip sonicator for 5 s with 1 s pulse at 20% amplitude and then passed through a 1 ml syringe with a 0.22 µm filter (Millipore Sigma). Neurons were incubated with 25 µM of DQ-BSA Red solution diluted into neuronal media for 2 h at 37°C. After DQ-BSA Red treatment, neurons were fixed in 4% PFA/4% sucrose solution in PBS at room temperature for 30 min. Neurons were then rinsed 3 times with PBS and incubated in Hoechst 33342 for 30 min at room temperature. Neurons were rinsed twice in PBS and mounted with Prolong Gold (Invitrogen). Coverslips were imaged on Zeiss Axiovert.Z1 widefield microscope at 63× oil objective.

DQ-BSA red analysis

In ImageJ, ROIs were drawn around the cell bodies. Hoechst 33342 staining was used as a guide to eliminate unhealthy or dead cells. Five fields were imaged per coverslip. Within each field, the corrected total cell fluorescence of an average of 5-15 cells was quantified per field as described in Marwaha and Sharma (2017). The mean corrected total cell fluorescence of all replicates for each sample was graphed.

Internalization assay

The neuronal uptake of PFFs was determined by conducting an internalization assay with Alexa-488-labeled fibrils as previously described (Froula et al., 2019). Primary hippocampal neurons were incubated for 30 min at 4°C in cold PBS with α-syn–Alexa-488 fibrils (0.1 µg/ml). This allowed binding to the plasma membrane. Neurons were relocated to incubate at 37°C which caused internalization for 30 min. Extracellular fibrils were quenched with trypan blue (1 mM). Images were captured using a Zeiss Axiovert.Z1 widefield microscope at 63× oil objective at an excitation/emission wavelength of 470/550 nm for fibrils and 560/630 nm for trypan blue. The median intensity of each frame captured was quantified using Zen 2.3 software (Carl Zeiss Microscopy, 2011) and normalized to the fluorescence intensity signal from trypan blue that was bound to the neuronal membrane.

Magic red cathepsin B activity assay

A magic red Cathepsin-B (CatB) assay (Immunochemistry Technology SKU: 937). This assay functions by measuring the fluorescence caused by CatB cleaving the magic red substrate. The protocol was adapted from the product manual under "Microscopy analysis of adherent cells." To elaborate, the magic red substrate was reconstituted with 50 µl of DMSO to generate a 250× stock staining solution. The stock was then diluted again to 25× in cell culture grade water (Fisher Scientific catalog #SH30529FS); 480 µl of water (DMSO or eliglustat, 100 nM) and 20 µl of 25× staining solution (1× final concentration) was added to each Mattek dish. Cells were incubated at 37°C for 35 min. Neurons were then rinsed twice with PBS with the second wash containing Hoechst 33342 (0.5% v/v) for 1 min incubation for the first wash followed by a 20 min incubation. Neurons were then fixed with 4% PFA, 4% sucrose solution for 30 min and were imaged in 1× PBS and 0.05% Saponin solution. Images were acquired and analyzed the same as DQ-BSA assay.

Sphingolipid quantification

Lipid extraction. Extraction of sphingolipids in cells was performed as described previously (Cosden et al., 2021). Briefly, primary cortical neurons were provided as frozen monolayers in 96-well plates. Extraction was performed within sample wells by addition of 150 µl MeOH spiked with a mix of stable isotopically labeled synthetic standards: d3 GlcCer d18:1/16:0, $^{13}C_6$ GlcSph 1-(β-D-glucosyl-1,2,3,4,5,6-13C6)-sphingosine (Matreya), d7 ceramide d18:1/16:0, d7 sphingosine, d7 sphingosine-1-phosphate and d9 sphingomyelin d18:/18:0 (Avanti Polar Lipids) at a final concentration of 10 ng/ml. Plates were capped, shaken for 10 min at room temperature, and centrifuged at 1500 × *g* for 5 min before the transfer of supernatants to new 96-well plates for mass spectrometry analyses.

Plasma sphingolipid extraction was performed using CHCl3:CH3OH (1:2) buffer spiked with 0.5 ng/ml of the SIL lipid standard mix from above. 0.4 ml of extraction buffer was mixed with 20 µl of plasma, shaken for 10 min at room temperature, and centrifuged at 3000 × *g* for 10 min; 300 µl of supernatant was removed and dried down using N_2 evaporation. Dried samples were reconstituted in 50 µl methanol immediately before analyses by mass spectrometry.

Extraction of glycosphingolipids from brain homogenates was adapted from the method established previously (Hamler et al., 2017). Brain homogenates were prepared from preweighed frozen tissue sections by addition of MeOH:H_2O (1:1) to generate an equivalent wet weight to volume ratio. Homogenization was performed at 200 oscillations/min for 2 min using a QIAGEN TissueLyser II bead mill (QIAGEN). $^{13}C_6$ GlcSph and d5 GlcCer d18:1/18:0 (Avanti) internal standards were prepared as a DMSO stock solution at 2 µg/ml and 0.02 µg/ml, respectively; 25 µl of the internal standard stock solution was added to 100 µl of homogenate before the addition of 400 µl of acetone/MeOH buffer (1:3). Extracts were shaken for 3 min, resuspended with 100 µl of water and centrifuged at 4000 × *g* for 10 min; 500 µl of supernatant was removed, combined with 200 µl MeOH:H_2O (1:1), and subjected to prefractionation via C18 solid phase extraction (SPE isolute C18, Biotage). SPE eluates were evaporated to dryness under N_2 gas and reconstituted in 50 µl DMSO and 200 µl mobile Phase B liquid chromatography buffer (see below).

Mass spectrometry. Sphingolipids were quantified by liquid chromatography mass spectrometry using multiple reaction monitoring scanning acquisition as described previously (Rocha et al., 2020). Separation was performed with a HALO HILIC 2.7 mm column (Advanced Materials Technology) using a Waters Acquity UPLC. Mobile Phase A and B consisted of 0.1% formic acid in H_2O and 95% acetonitrile, 2.5% MeOH, 2.0% H_2O, 0.5% formic acid, and 5 mM ammonium formate, respectively. A 10 min gradient was sufficient to achieve baseline separation of endogenous isomeric lipid species, such as GlcSph and galactosylsphingosine. Multiple reaction monitoring acquisition was performed with a SciEx 5500 QTRAP mass spectrometer operating in positive ion mode. Lipid quantification from primary cortical neurons was reported as ratios to internal standard and was used to compare relative changes in abundances across conditions. Absolute quantification was performed in plasma and brain tissue specimens using standard curves for each targeted species. For plasma lipid quantification, serial dilutions of a stock solution of 5 μg/ml of d5 GlcCer d18:1/18:0, ceramide d18:1/16:0, sphingosine d18:1, sphingosine-1-phosphate d18:1, sphingomyelin (porcine brain std; Avanti) and 50 ng/ml of GlcSph d18:1 (Avanti) were processed as plasma above, and standard curves were generated within each study plate. Absolute quantification of brain GlcCers was performed in tissue homogenates by spiking in serial dilutions down to 1/1000 of the d5 GlcCer d18:1/18:0 (1 mg/ml) stock solution for analysis as above. GlcSph standard curves were generated using serial dilutions GlcSph d18:1 standard (Avanti) from DMSO stocks processed as above for LC-MS/MS analyses. Linear calibration curves with $1/x^2$ weighting factor were generated by plotting the ratio of the peak area of standards to internals standards. Total GlcCer was represented as the sum concentrations of C16:0 through C24:1 chain length variants.

GCase activity assay

$GBA1^{+/+}$ and $GBA1^{+/L444P}$ mice were perfused with 30-40 ml of 0.9% NaCl saline (with 0.5% w/v sodium nitroprusside and 10 units/ml heparin) at 2 months of age. The brain was removed and dissected to isolate the midbrain, hippocampus, striatum, and cortex. Tissue samples were homogenized with a mini handheld homogenizer in lysis buffer (50 mM Tris, 150 mM NaCl, 5 mM EDTA, 1% Triton X-100, 0.1% sodium deoxycholate) and centrifuged for 10 min at 5000 × *g*. The Pierce BCA Protein Assay Kit (Fisher Scientific catalog #23225) was used to determine the protein concentration of the supernatant of each sample.

The measurement of GCase activity in each homogenate sample was performed as previously described (Arrant et al., 2019). Each sample was diluted to 1 mg/ml in citrate PB (0.1 M sodium citrate dihydrate, 0.2 M sodium phosphate monohydrate), such that 5 μg of protein (5 μl) was loaded in pentaplicate into a black, clear-bottom 96-well plate. GCase assay buffer (citrate PB with 1% BSA, 0.25% Triton X-100, 0.25% taurocholic acid, and 1.11 mM EDTA at pH 4.6) containing either 4-methylumbelliferone β-D-glucopyranoside (4-MUGluc, 1.11 mM) or 4-MUGluc and conduritol B epoxide (CBE, 0.2 mM) was added to each well at 45 μl such that three wells contained 4-MUGluc and two wells contained 4-MUGluc and CBE in a final volume of 50 μl. Each plate was analyzed with a set of blanks (no protein) to determine the background signal of 4-MUGluc, 4-MUGluc, and CBE. Reaction plates were incubated at 37°C for 1 h, after which 50 μl of stop solution (0.4 M glycine, pH 11) was added to each well. Standard dilutions of 4-MU, eight concentrations ranging from 0 to 7.5 μM in 100 μl of 50% assay buffer and 50% stop solution, were added to each plate in duplicate. Fluorescence intensity was recorded on a Synergy 2 plate reader (BioTek) at ex/em wavelengths of 360 nm/440 nm.

Specific GCase activity was determined for each sample by correcting for background fluorescence and the fluorescent signal produced in the presence of the GCase inhibitor, CBE. The corrected fluorescent signal of each sample was then compared with the standard curve of 4-MU to determine the nmol 4-MU produced per hour per milligram of protein loaded. GCase activity was determined for the midbrain, hippocampus, striatum, and frontal cortex of 8 $GBA1^{+/+}$ (6 M:2 F) and 8 $GBA1^{+/L444P}$ mice (6 M:2 F)

Immunoblotting

At 3 months of age, $GBA1^{+/+}$ and $GBA1^{+/L444P}$ mice were transcardially perfused with 0.9% NaCl saline. The brain was removed and dissected to isolate the midbrain, hippocampus, striatum, and cortex. The tissues were homogenized with a mini handheld homogenizer in homogenization buffer (1% Triton X-100, protease inhibitor, and phosphatase inhibitor in TBS). Samples were centrifuged at 4°C for 30 min at 21,150 × *g* and supernatant was collected. The Pierce BCA Protein Assay Kit (Fisher Scientific catalog #23225) was used to determine the protein concentration of the supernatant of each sample.

Protein sample was loaded into each well of a 4%-20% Mini-PROTEAN TGX Precast protein 15-well gels (Bio-Rad, catalog #4561096). Protein was transferred using transfer buffer (20% MeOH in TBS) to a PVDF membrane overnight at 4°C at 25 V. The next day, membranes were rinsed 3 times with TBS/1%Tween followed by 1 h blocking using the Intercept (TBS) Blocking Buffer and Diluent Kit (LI-COR, catalog #927-66003). After the membranes were rinsed 3 times using TBS-Tween, membranes were incubated in a primary solution from the diluent kit indicated above.

Primary antibodies used were as indicated: vinculin (Bio-Rad catalog #MCA465GA, alternatively, catalog #MCA465S, RRID:AB_2214389), GCase (Sigma-Aldrich catalog #G4171, RRID:AB_1078958), total α-syn (Abcam catalog #ab51252, RRID:AB_869971), p-α-syn (Abcam, catalog #ab51253, RRID:AB_869973), vGLUT1 (Synaptic Systems, catalog #135304, RRID:AB_887878), Homer1 (Synaptic Systems catalog #160006, RRID:AB_2631222), Tuj1 (Neuromics catalog #MO15013, RRID:AB_2737114), SNAP25 (Sigma-Aldrich catalog #S9684, RRID:AB_261576), VAMP2 (Synaptic Systems catalog #104211, RRID:AB_887811), and syntaxin-1a (Sigma-Aldrich catalog #SAB4502894, RRID:AB_10748204). After the membranes were incubated at 4°C overnight, membranes were rinsed 3 times and then incubated in a secondary solution for 1 h with the secondary diluent kit as indicated above. SDS was added to generate 0.01% SDS secondary antibody solution. The secondary antibodies were as indicated: IRDye 800CW Goat anti-Rabbit IgG Secondary Antibody (LI-COR Biosciences catalog #925-32211, RRID:AB_2651127), IRDye 680RD Donkey anti-Guinea Pig IgG Secondary Antibody (LI-COR Biosciences catalog #926-68077, RRID:AB_10956079), IRDye 800CW Donkey anti-Chicken Secondary Antibody (LI-COR Biosciences catalog #926-32218, RRID:AB_1850023), and AlexaFluor-680 anti-Mouse IgG Secondary Antibody. Bands were imaged and analyzed, by quantifying band intensity, using Image Studio Lite version 5.2. The band of the protein of interest was normalized to the loading control, vinculin. All immunoblots were run with 3-6 individual mice.

Statistical analysis

All data were graphed with GraphPad Prism 9 and analyzed with the ROUT test for outliers at Q = 10% then tested for normality using the Shapiro–Wilks test. Data that failed the test for normality were graphed as a scatter plot without a bar using a Mann–Whitney test. If data were normal, an independent *t* test, two-way ANOVA, or three-way ANOVA were used. All data are presented as mean ± SEM A $p < 0.05$ was considered statistically significant. A list of the statistical tests used for each graph can be found in Table 1.

Results

Fibril-induced α-syn inclusion formation in primary cultured hippocampal neurons from $GBA1^{+/+}$ and $GBA1^{+/L444P}$ mice

To study the effects of GBA1L444P expression on α-syn inclusion formation, we first used primary hippocampal neurons from $GBA1^{+/+}$ mice and $GBA1^{+/L444P}$ knock-in mice exposed to short α-syn fibrils on DIV7 and analyzed 14 d later (DIV21) (Volpicelli-Daley et al., 2011). Primary hippocampal neurons from mice were chosen as our model culture system because we achieve reliable, robust formation of α-syn inclusions in response to exposure to fibrils (Volpicelli-Daley et al., 2014; Froula et al., 2018; Brzozowski et al., 2021; Stoyka et al., 2021). Because the formation of α-syn inclusions depends on levels of synaptic α-syn and thus neuronal development (Murphy et al., 2000), we

Table 1. Statistical test describing the figure, data, type of test, and statistical results

Figure	Description of graph location	Statistical test	Descriptive statistics
1*B*	Percent area of NF (left) and p-α-syn (right)	Nested two-way ANOVA via SPSS	Neurofilament:
		Descriptive statistics acquired from GraphPad Prism	Interaction: $F_{(1,48)} = 1.045$, $p = 0.3117$
			Drug treatment: $F_{(1,48)} = 0.1011$, $p = 0.7519$
			Genotype: $F_{(1,48)} = 0.7340$, $p = 0.3959$
			p-α-syn:
			Interaction: $F_{(1,48)} = 1.838$, $p = 0.1815$
			Drug treatment: $F_{(1,48)} = 0.8887$, $p = 0.3506$
			Genotype: $F_{(1,48)} = 20.29$, ****$p < 0.0001$
1*D*	DQ-BSA	Three-way ANOVA	Interaction: $F_{(1,18)} = 3.621$, $p = 0.0732$
			Drug treatment × α-syn treatment: $F_{(1,18)} = 7.092$, *$p = 0.0158$
			Drug treatment × genotype: $F_{(1,18)} = 9.580$ **$p = 0.0062$
			α-syn treatment × genotype: $F_{(1,18)} = 2.512$, $p = 0.1304$
			Drug treatment: $F_{(1,18)} = 10.41$, **$p = 0.0047$
			α-syn treatment: $F_{(1,18)} = 1.966$, $p = 0.1778$
			Genotype: $F_{(1,18)} = 6.234$, *$p = 0.0225$
2*A*	GCase activity assay	Independent *t* test	Cortex: $t_{(10)} = 7.406$, ****$p < 0.0001$
			Striatum: $t_{(10)} = 3.023$, *$p = 0.0128$
			Hippocampus: $t_{(10)} = 6.870$, ****$p < 0.0001$
			Midbrain: $t_{(10)} = 4.593$, ***$p < 0.0010$
2*C*	Western blot: GCase (left), total synuclein (middle), p-α-syn (right)	Independent *t* test	GCase:
		Mann–Whitney test	$t_{(4)} = 1.093$, $p = 0.3360$
		Failed Shapiro–Wilk test	Total synuclein:
			W = 4, $p = 0.9999$
		Independent *t* test	p-α-syn:
			$t_{(9)} = 2.808$; *$p = 0.0205$
2*D*	Western blot: vGlut1 (left), Homer1 (middle), Tuj1 (right)	Independent *t* test	vGlut1:
			$t_{(5)} = 6.686$; **$p = 0.0011$
			Homer1:
			$t_{(4)} = 1.481$; $p = 0.2127$
			Tuj1:
			$t_{(9)} = 0.05656$, $p = 0.9561$
2*E*	Western blot: SNAP25 (left), VAMP2 (middle), Syntaxin1a (right)	Independent *t* test	SNAP25:
			$t_{(5)} = 0005117$, $p = 0.9996$
			VAMP2:
			$t_{(4)} = 1.433$, $p = 0.2251$
			Syntaxin1a:
			$t_{(6)} = 0.3713$, $p = 0.7232$
3*A*	Open field test	Independent *t* test	Average velocity:
			$t_{(10)} = 2.002$, $p = 0.0732$
			Percent in center:
			$t_{(11)} = 1.436$, $p = 0.1790$
			Distance traveled:
			$t_{(10)} = 1.243$, $p = 0.2424$
3*B*	Pole test	Independent *t* test	Total descent time:
			$t_{(10)} = 2.638$, *$p = 0.0248$
			Turnaround time:
			$t_{(12)} = 0.2243$, $p = 0.8263$
			Time descending:
			$t_{(11)} = 1.467$, $p = 0.1704$
3*C*	Training	Repeated-measures two-way ANOVA	Time: $F_{(4, 48)} = 49.13$, ****$p < 0.0001$
			Genotype: $F_{(1, 12)} = 1.106$, $p = 0.3136$
			Time × genotype: $F_{(4, 48)} = 2.751$, *$p = 0.0386$
3*C*	Cued and contextual fear conditioning	Independent *t* test	Contextual:
			$t_{(11)} = 2.720$, *$p = 0.0199$
			Cued:
			$t_{(12)} = 2.069$, $p = 0.0608$
4*A*	GlcSph	Two-way ANOVA	Interaction: $F_{(3,50)} = 2.270$, $p = 0.0918$
			Age: $F_{(3,50)} = 23.54$, $p < 0.0001$
			Genotype: $F_{(1,50)} = 64.23$, $p < 0.0001$
4*B*	Total GlcCer	Two-way ANOVA	Interaction: $F_{(3,50)} = 1.454$, $p = 0.2384$
			Age: $F_{(3,50)} = 3.340$, $p = 0.0265$
			Genotype: $F_{(1,50)} = 2.493$, $p = 0.1206$
4*C*	GlcSph	Independent *t* test	$t_{(9)} = 2.810$, *$p = 0.0204$
4*D*	GlcCer	Independent *t* test	$t_{(10)} = 1.015$, $p = 0.3338$

(*Table continues*.)

Table 1. Continued

Figure	Description of graph location	Statistical test	Descriptive statistics
5*B*	PFC	Two-way ANOVA	Interaction: $F_{(1,16)} = 6.890$, $p = 0.0184$ Drug treatment: $F_{(1,16)} = 13.95$, $^{**}p = 0.0018$ Genotype: $F_{(1,16)} = 1.842$, $p = 0.1936$
5*D*	DG: granule cell layer CA1 pyramidal cell layer CA2-CA3 pyramidal cell layer	Two-way ANOVA Independent *t* test	Interaction: $F_{(1,16)} = 7.484$, $p = 0.0147$ Drug treatment: $F_{(1,16)} = 0.05575$, $p = 0.8163$ Genotype: $F_{(1,16)} = 23.18$, $p = 0.0002$ CA1 pyramidal cell layer: $t_{(11)} = 2.580$; $^{*}p = 0.0256$ CA2-CA3 pyramidal cell layer: $t_{(13)} = 1.997$; $p = 0.0672$
5*F*	SNc	Two-way ANOVA	Interaction: $F_{(1,19)} = 0.6662$, $p = 0.4245$ Drug treatment: $F_{(1,19)} = 0.02359$, $p = 0.8795$ Genotype: $F_{(1,19)} = 1.459$, $p = 0.2420$
6*C*	Estimated cell population	Three-way ANOVA	Interaction: $F_{(1,34)} = 0.06097$, $p = 0.8065$ Drug treatment × α-syn treatment: $F_{(1,34)} = 0.2240$, $p = 0.6390$ Drug treatment × genotype: $F_{(1,34)} = 0.06160$, $p = 0.8055$ α-syn treatment × genotype: $F_{(1,34)} = 0.0002467$, $p = 0.9876$ Drug treatment: $F_{(1,34)} = 4.451$ $^{*}p = 0.0423$ α-syn treatment: $F_{(1,34)} = 36.68$ $^{*}p < 0.0001$ Genotype: $F_{(1,34)} = 2.122$, $p = 0.1544$
7*A*	Survival curves	Kaplan–Meier survival curve	Post-monomer injection: Log-rank (Mantel–Cox) test: χ^2 (3, $N = 57$) = 8.722, $^{*}p = 0.0332$ Post-fibril injection: Log-rank (Mantel–Cox) test χ^2 (3, $N = 42$) = 0.6481, $p = 0.8853$
7*B*	Open field test	Three-way ANOVA	Distance traveled: Interaction: $F_{(1,66)} = 1.655$, $p = 0.2028$ Drug treatment × α-syn treatment: $F_{(1,66)} = 1.201$, $p = 0.2771$ Drug treatment × genotype: $F_{(1,66)} = 0.01696$, $p = 0.8968$ α-syn treatment × genotype: $F_{(1,66)} = 0.2655$, $p = 0.6081$ Drug treatment: $F_{(1,66)} = 2.578$, $p = 0.1131$ α-syn treatment: $F_{(1,66)} = 2.965$, $p = 0.0898$ Genotype: $F_{(1,66)} = 1.084$, $p = 0.3016$ Average velocity: Interaction: $F_{(1,66)} = 0.02006$, $p = 0.8878$ Drug treatment × α-syn treatment: $F_{(1,66)} = 0.7082$, $p = 0.4031$ Drug treatment × genotype: $F_{(1,66)} = 0.3206$, $p = 0.5732$ α-syn treatment × genotype: $F_{(1,66)} = 0.6204$, $p = 0.4337$ Drug treatment: $F_{(1,66)} = 5.121$, $p = 0.0269$ α-syn treatment: $F_{(1,66)} = 0.5298$, $p = 0.4693$ Genotype: $F_{(1,66)} = 0.05453$, $p = 0.8161$ Percent in center: Interaction: $F_{(1,70)} = 0.5531$, $p = 0.4596$ Drug treatment × α-syn treatment: $F_{(1,70)} = 0.0002562$, $p = 0.9873$ Drug treatment × genotype: $F_{(1,70)} = 1.246$, $p = 0.2681$ α-syn treatment × genotype: $F_{(1,70)} = 1.774$, $p = 0.1872$ Drug treatment: $F_{(1,70)} = 5.160$, $^{*}p = 0.0262$ α-syn treatment: $F_{(1,70)} = 0.5955$, $p = 0.4429$ Genotype: $F_{(1,70)} = 1.535$, $p = 0.2195$
7*C*	Pole test	Three-way ANOVA	Turnaround time: Interaction: $F_{(1,69)} = 2.500$, $p = 0.1184$ Drug treatment × α-syn treatment: $F_{(1,69)} = 0.8307$, $p = 0.3652$ Drug treatment × genotype: $F_{(1,69)} = 2.814$, $p = 0.0980$ α-syn treatment × genotype: $F_{(1,69)} = 0.4537$, $p = 0.5028$ Drug treatment: $F_{(1,69)} = 6.223$, $^{*}p = 0.0150$ α-syn treatment: $F_{(1,69)} = 5.396$, $^{*}p = 0.0231$ Genotype: $F_{(1,69)} = 0.1263$, $p = 0.7234$ Time descending: Interaction: $F_{(1,62)} = 0.2636$, $p = 0.6095$ Drug treatment × α-syn treatment: $F_{(1,62)} = 0.4947$, $p = 0.4845$ Drug treatment × genotype: $F_{(1,62)} = 0.3006$, $p = 0.5855$ α-syn treatment × genotype: $F_{(1,62)} = 0.3767$, $p = 0.5416$

(*Table continues*.)

Table 1. Continued

Figure	Description of graph location	Statistical test	Descriptive statistics
			Drug treatment: $F_{(1,62)} = 0.2163$, $p = 0.6435$ α-syn treatment: $F_{(1,62)} = 4.483$, $^{*}p = 0.0382$ Genotype: $F_{(1,62)} = 4.874$, $^{*}p = 0.0310$ Total descent time: Interaction: $F_{(1,62)} = 0.003431$, $p = 0.9535$ Drug treatment × α-syn treatment: $F_{(1,62)} = 0.8643$, $p = 0.3561$ Drug treatment × genotype: $F_{(1,62)} = 0.09758$, $p = 0.7558$ α-syn treatment × genotype: $F_{(1,62)} = 0.7574$, $p = 0.3875$ Drug treatment: $F_{(1,62)} = 3.983$, $p = 0.0504$ α-syn treatment: $F_{(1,62)} = 4.805$, $p = 0.0321$ Genotype: $F_{(1,62)} = 2.267$, $p = 0.1372$
7D	Training	Repeated-measures three-way ANOVA	Training: control Interaction: $F_{(4240)} = 0.6830$, $p = 0.6044$ Time × α-syn treatment: $F_{(4240)} = 4.425$, $^{**}p = 0.0018$ Time × genotype: $F_{(4240)} = 0.0877$, $p = 0.9862$ α-syn treatment × genotype: $F_{(1,60)} = 0.6170$, $p = 0.4353$ Time: $F_{(4240)} = 120.1$, $^{****}p < 0.0001$ α-syn treatment: $F_{(1,60)} = 2.12$, $p = 0.1506$ Genotype: $F_{(1,60)} = 0.4373$, $p = 0.5110$ Training: venglustat Interaction: $F_{(4,64)} = 0.5828$, $p = 0.6762$ Time × α-syn treatment: $F_{(4,64)} = 0.5808$, $p = 0.6776$ Time × genotype: $F_{(4,64)} = 0.8026$, $p = 0.5280$ α-syn treatment × genotype: $F_{(1,16)} = 0.1628$, $p = 0.6919$ Time: $F_{(2.882,46.11)} = 25.40$, $^{****}p < 0.0001$ α-syn treatment: $F_{(1,16)} = 0.006116$, $p = 0.9386$ Genotype: $F_{(1,16)} = 1.846$, $p = 0.1931$
7E	Cued and contextual fear conditioning	Three-way ANOVA	Cued: Interaction: $F_{(1,76)} = 0.03063$, $p = 0.8615$ Drug treatment × α-syn treatment: $F_{(1,76)} = 1.378$, $p = 0.2441$ Drug treatment × genotype: $F_{(1,76)} = 1.865$, $p = 0.1761$ α-syn treatment × genotype: $F_{(1,76)} = 0.6219$, $p = 0.4328$ Drug treatment: $F_{(1,76)} = 1.757$, $p = 0.1890$ α-syn treatment: $F_{(1,76)} = 5.703$, $^{*}p = 0.0194$ Genotype: $F_{(1,76)} = 1.960$, $p = 0.1656$ Contextual: Interaction: $F_{(1,76)} = 0.07405$, $p = 0.7863$ Drug treatment × α-syn treatment: $F_{(1,76)} = 0.07986$, $p = 0.7783$ Drug treatment × genotype: $F_{(1,76)} = 0.3424$, $p = 0.5602$ α-syn treatment × genotype: $F_{(1,76)} = 0.2234$, $p = 0.6378$ Drug treatment: $F_{(1,76)} = 0.0002150$, $p = 0.9883$ α-syn treatment: $F_{(1,76)} = 1.850$, $p = 0.1778$ Genotype: $F_{(1,76)} = 3.979$, $^{*}p = 0.0497$
Extended Data Figure 1-1*B*	Percent area of NF (left) and p-α-syn (right)	Two-way ANOVA	Neurofilament: Interaction: $F_{(1,16)} = 0.4965$, $p = 0.4912$ Drug treatment: $F_{(1,16)} = 0.2427$, $p = 0.6290$ Genotype: $F_{(1,16)} = 0.01635$, $p = 0.8999$ p-α-syn: Interaction: $F_{(1,16)} = 0.007994$, $p = 0.9299$ Drug treatment: $F_{(1,16)} = 0.09064$, $p = 0.7672$ Genotype: $F_{(1,16)} = 0.5849$, $p = 0.4555$
Extended Data Figure 1-2*A*	GlcCer	Three-way ANOVA	Interaction: $F_{(3151)} = 1.524$, $p = 0.2106$ Dose × α-syn treatment: $F_{(3151)} = 0.3454$, $p = 0.7926$ Dose × genotype: $F_{(3151)} = 0.7284$, $p = 0.5365$ Genotype × α-syn treatment: $F_{(1151)} = 3.856$, $p = 0.0514$ Dose: $F_{(3151)} = 28.06$, $^{****}p < 0.0001$ α-syn treatment: $F_{(1151)} = 1.454$, $p = 0.2299$ Genotype: $F_{(1151)} = 0.1898$, $p = 0.6637$
Extended Data Figure 1-2*B*	Sphingomyelin	Three-way ANOVA	Interaction: $F_{(3151)} = 0.2265$, $p = 0.8778$ Dose × α-syn treatment: $F_{(3151)} = 0.3922$, $p = 0.7588$ Dose × genotype: $F_{(3151)} = 0.3684$, $p = 0.7759$ Genotype × α-syn treatment: $F_{(1151)} = 0.7365$, $p = 0.3921$ Dose: $F_{(3151)} = 11.11$, $^{****}p < 0.0001$

(*Table continues*.)

Table 1. Continued

Figure	Description of graph location	Statistical test	Descriptive statistics
			α-syn treatment: $F_{(1151)} = 0.6928$, $p = 0.4065$ Genotype: $F_{(1151)} = 0.08458$, $p = 0.7716$
Extended Data Figure 1-2C	Sphingosine	Three-way ANOVA	Interaction: $F_{(3157)} = 1.152$, $p = 0.3302$ Dose × α-syn treatment: $F_{(3157)} = 0.4860$, $p = 0.6925$ Dose × genotype: $F_{(3157)} = 1.166$, $p = 0.3245$ Genotype × α-syn treatment: $F_{(1157)} = 1.259$, $p = 0.2636$ Dose: $F_{(3157)} = 1.922$, $p = 0.1283$ α-syn treatment: $F_{(1157)} = 0.05604$, $p = 0.8132$ Genotype: $F_{(1157)} = 0.5954$, $p = 0.4415$
Extended Data Figure 1-2D	Ceramide	Three-way ANOVA	Interaction: $F_{(3151)} = 1.515$, $p = 0.2128$ Dose × α-syn treatment: $F_{(3151)} = 0.2502$, $p = 0.8611$ Dose × genotype: $F_{(3151)} = 0.2116$, $p = 0.8882$ Genotype × α-syn treatment: $F_{(1151)} = 5.610$, $^{*}p = 0.0191$ Dose: $F_{(3151)} = 4.115$, $^{**}p = 0.0077$ α-syn treatment: $F_{(1151)} = 0.01056$, $p = 0.9183$ Genotype: $F_{(1151)} = 0.08041$, $p = 0.7771$
Extended Data Figure 1-3B	Internalization of PFF-488	Two-way ANOVA	Interaction: $F_{(1,6)} = 0.3480$, $p = 0.5768$ Drug treatment: $F_{(1,6)} = 0.07183$, $p = 0.7977$ Genotype: $F_{(1,6)} = 0.03039$, $p = 0.8673$
Extended Data Figure 1-4B	Total α-synuclein at DIV7 (left) and DIV21 (right)	Independent *t* test	DIV7: $t_{(3)} = 0.3553$, $p = 0.7459$ DIV21: $t_{(5)} = 0.04483$, $p = 0.9660$
Extended Data Figure 1-4D	Total α-synuclein	Two-way ANOVA	Interaction: $F_{(1,2)} = 0.005705$, $p = 0.9467$ Drug treatment: $F_{(1,2)} = 0.3405$, $p = 0.6186$ Genotype: $F_{(1,2)} = 3.430$, $p = 0.2052$
Extended Data Figure 1-5B	CatB activity	Nested two-way ANOVA	Interaction: $F_{(1,51)} = 2.758$, $p = 0.1029$ Drug treatment: $F_{(1,51)} = 10.27$, $^{**}p = 0.0023$ Genotype: $F_{(1,51)} = 7.014$, $^{*}p = 0.0107$
Extended Data Figure 4-1A	GlcCer C18:0	Two-way ANOVA	Interaction: $F_{(3,50)} = 2.173$, $p = 0.1028$ Age: $F_{(3,50)} = 12.77$, $p < 0.0001$ Genotype: $F_{(1,50)} = 0.2353$, $p = 0.6297$
Extended Data Figure 4-1B	GlcCer C20:0	Two-way ANOVA	Interaction: $F_{(3,48)} = 0.6806$, $p = 0.5682$ Age: $F_{(3,48)} = 0.7990$, $p = 0.5005$ Genotype: $F_{(1,48)} = 1.619$, $p = 0.2094$
Extended Data Figure 4-1C	GlcCer C22:0	Two-way ANOVA	Interaction: $F_{(3,50)} = 0.3007$, $p = 0.8247$ Age: $F_{(3,50)} = 1.027$, $p = 0.3886$ Genotype: $F_{(1,50)} = 2.898$, $p = 0.0949$
Extended Data Figure 4-1D	GlcCer C24:1	Two-way ANOVA	Interaction: $F_{(3,50)} = 0.7606$, $p = 0.5215$ Age: $F_{(3,50)} = 1.821$, $p = 0.1554$ Genotype: $F_{(1,50)} = 9.377$, $^{**}p = 0.0035$
Extended Data Figure 5-1A	Aggregate burden of the amygdala	Mann–Whitney Test Failed Shapiro–Wilk test	$W = 11$, $p = 0.1690$
Extended Data Figure 5-1B	Aggregate burden of the entorhinal cortex	Independent *t* test	$t_{(11)} = 0.03628$; $p = 0.9717$
Extended Data Figure 5-1C	Ceramide	Three-way ANOVA	Interaction: $F_{(1,35)} = 0.9955$, $p = 0.3253$ Drug treatment × α-syn treatment: $F_{(1,35)} = 2.536$, $p = 0.1203$ Drug treatment × genotype: $F_{(1,35)} = 5.255$, $^{*}p = 0.0280$ α-syn treatment × genotype: $F_{(1,35)} = 0.6352$, $p = 0.4308$ Drug treatment: $F_{(1,35)} = 7.185$, $^{*}p = 0.0111$ α-syn treatment: $F_{(1,35)} = 1.582$, $p = 0.2168$ Genotype: $F_{(1,35)} = 7.241$, $^{*}p = 0.0109$
Extended Data Figure 5-2D	Sphingomyelin	Three-way ANOVA	Interaction: $F_{(1,35)} = 7.734$, $^{**}p = 0.0087$ Drug treatment × α-syn treatment: $F_{(1,35)} = 3.327$, $p = 0.0767$ Drug treatment × genotype: $F_{(1,35)} = 3.289$, $p = 0.0783$ α-syn treatment × genotype: $F_{(1,35)} = 8.184$, $^{**}p = 0.0071$ Drug treatment: $F_{(1,35)} = 24.29$, $^{****}p < 0.0001$ α-syn treatment: $F_{(1,35)} = 0.7393$, $p = 0.3957$ Genotype: $F_{(1,35)} = 2.626$, $p = 1141$
Extended Data Figure 5-2E	Sphingosine-1-phosphate	Three-way ANOVA	Interaction: $F_{(1,32)} = 0.008874$, $p = 0.9255$ Drug treatment × α-syn treatment: $F_{(1,32)} = 3.188$, $p = 0.0836$ Drug treatment × genotype: $F_{(1,32)} = 0.04317$, $p = 0.8367$ α-syn treatment × genotype: $F_{(1,32)} = 0.6178$, $p = 0.4376$ Drug treatment: $F_{(1,32)} = 1.016$, $p = 0.3209$

(*Table continues*.)

Table 1. Continued

Figure	Description of graph location	Statistical test	Descriptive statistics
			α-syn treatment: $F_{(1,32)} = 9.109$, $^{**}p = 0.0050$
			Genotype: $F_{(1,32)} = 0.1771$, $p = 0.6767$
Extended Data Figure 5-3	NeuN count: dmPFC	Two-way ANOVA	Interaction: $F_{(1,16)} = 0.07678$, $p = 0.7853$
			Drug treatment: $F_{(1,16)} = 0.02827$, $p = 0.8686$
			Genotype: $F_{(1,16)} = 2.821$, $p = 0.1124$
Extended Data Figure 5-5	Total α-syn expression	Two-way ANOVA	Interaction: $F_{(3,16)} = 0.01274$, $p = 0.9979$
			Brain region: $F_{(3,16)} = 0.4320$, $p = 0.7329$
			Genotype: $F_{(1,16)} = 0.007856$, $p = 0.9305$

quantified axonal density using neurofilament-H (heavy polypeptide) to ensure there were no differences in the overall axonal outgrowth. There was no change in the percent area occupied by neurofilament-H(NF) in neurons from GBA1$^{+/L444P}$ mice compared with GBA1$^{+/+}$ neurons with and without fibrils (Fig.1*A*,*B*, left, DMSO: $p = 0.9996$; Eliglustat: $p = 0.2632$). Fourteen days after exposure to fibrils, α-syn phosphorylated at Serine129 (p-α-syn), which is used as a marker of inclusion formation, was not significantly different between DMSO-treated neurons from GBA1$^{+/L444P}$ or GBA1$^{+/+}$ mice (Fig.1*A*,*B*, right, DMSO: $p = 0.2149$; Eliglustat: $p < 0.0001$). The percent area of p-α-syn was normalized by dividing by the percent area occupied by neurofilament-H IF. To determine whether p-α-syn was altered at an earlier time point, neurons were evaluated at DIV14, 7 d after exposure to fibrils. Hippocampal neurons showed no difference in abundance of p-α-syn inclusions between genotype or drug treatment (Extended Data Fig. 1-1). Accordingly, DIV21 was used for all primary culture experiments. Quantitation of sphingolipids by mass spectrometry in the primary neuronal cultures showed no differences in levels of GlcCer, total sphingomyelin, sphingosine, or ceramide in neurons exposed to fibrils compared with no treatment, or in neurons expressing GBA1$^{+/L444P}$ compared with GBA1$^{+/+}$ (Extended Data Fig. 1-2*A-D*). GlcSph was not detectable in the primary neuronal cultures.

Because it has been proposed that mutant *GBA1* increases α-syn aggregation by increasing levels of GlcCer (Mazzulli et al., 2011; Stojkovska et al., 2018), primary hippocampal neurons were treated with eliglustat which prevents the formation of GlcCer and GlcSph by inhibiting GCS (Bennett and Turcotte, 2015). Neurons were treated with 1, 10, and 100 nM eliglustat (IC_{50} = 20 nM of intact MDCK cells) (Shayman, 2010), and mass spectrometry quantitation of lipids showed that 100 nM of eliglustat significantly reduced levels of total GlcCer, with no effect on total sphingomyelins, sphingosine, or ceramide (Extended Data Fig. 1-2*A-D*). Fourteen days of treatment with eliglustat did not alter axon density as seen with NF IF (Fig. 1*A*,*B*, left). However, 14 d of eliglustat treatment significantly increased the abundance of fibril-induced α-syn inclusions in primary neurons from GBA1$^{+/L444P}$ mice compared with neurons from GBA1$^{+/+}$ mice (Fig. 1*A*,*B*, right). Eliglustat did not alter neuronal uptake of fibrils (Extended Data Fig. 1-3). Because the presence of pathologic α-syn depends on the levels of endogenous total α-syn, total α-syn was quantified by immunoblot. There were no statistical differences in α-syn levels between neurons expressing GBA1$^{+/L444P}$ compared with GBA1$^{+/+}$ at DIV7 or DIV21 or between drug treatment 14 d after treatment (Extended Data Fig. 1-4).

Lysosome function in primary cultured hippocampal neurons from GBA1$^{+/+}$ mice or GBA1$^{+/L444P}$ mice with and without fibrils

GCase activity plays a role in lysosome function (Boer et al., 2020). Thus, a DQ-BSA assay was used to determine the impact of GBA1L444P on late endosomes/lysosome activity in neurons. According to this assay, active proteases in these organelles cleave DQ-BSA, which then fluoresces (Fig. 1*C*,*D*). Primary neurons from GBA1$^{+/L444P}$ mice showed significantly reduced DQ-BSA fluorescence compared with neurons from GBA1$^{+/+}$ mice. In addition, 14 d of fibril exposure significantly reduced DQ-BSA fluorescence in neurons from GBA1$^{+/+}$ mice compared with neurons from GBA1$^{+/+}$ mice not exposed to fibrils. Fibril exposure did not further reduce DQ-BSA fluorescence in neurons from GBA1$^{+/L444P}$ mice compared with GBA1$^{+/+}$ mice. Eliglustat-treated primary neurons showed significantly reduced DQ-BSA fluorescence compared with GBA1$^{+/+}$ control neurons. Thus, while both expressions of GBA1L444P and exposure to fibrils reduced late endosome/lysosome activity, eliglustat treatment and reduction of GlcCer did not rescue these impairments. To further evaluate lysosomal function in this GBA1-PD model, primary hippocampal neurons from GBA1$^{+/+}$ and GBA1$^{+/L444P}$ mice underwent the Magic Red CatB Activity assay. CatB is a common lysosomal protease that is also seen to be a risk factor for GBA1-PD (Blauwendraat et al., 2020). Neurons were only treated with eliglustat or equal volumes of DMSO. Interestingly, eliglustat-treated GBA1$^{+/L444P}$ neurons showed an increase in CatB activity compared with control groups (Extended Data Fig. 1-5). Overall, generalized lysosomal protease activity, as determined by the DQ-BSA assay, is reduced, whereas CatB activity, specifically, is increased solely in eliglustat-treated GBA1$^{+/L444P}$ neurons.

Expression of synaptic proteins and behavior in GBA1$^{+/L444P}$ mice compared with GBA1$^{+/+}$ mice

Because there are few studies characterizing baseline behavior and possible changes in the brains of GBA1$^{+/L444P}$ mice, analyses of levels of neuronal protein expression and behavior in 3-month-old GBA1$^{+/L444P}$ mice compared with GBA1$^{+/+}$ mice without fibrils or any stereotactic injections was performed. The cortex, striatum, hippocampus, and midbrain were analyzed. All regions showed reduced GCase activity in GBA1$^{+/L444P}$ mice compared with GBA1$^{+/+}$ mice. The reduction of GCase activity, as measured by the 4-MU assay, was 31.9% in the cortex, 21.6% in the striatum, 27.4% in the hippocampus, and 27.7% in the midbrain (Fig. 2*A*). Hippocampal brain lysates were used to evaluate neuronal protein expression. There was no change in the expression of levels of GCase protein (Fig. 2*B*,*C*). In addition, there were no changes in levels of total synuclein, but rather a reduction in soluble p-α-syn between the GBA1$^{+/+}$ and GBA1$^{+/L444P}$ mice (Fig. 2*B*,*C*). Hippocampal levels of synaptic and neuronal proteins were also analyzed. Levels of presynaptic vGLUT1, which transports glutamate into synaptic vesicles, were significantly reduced in the GBA1$^{+/L444P}$ mice (Fig. 2*B*,*D*) compared with GBA1$^{+/+}$ mice. Levels of neuron-specific Tuj1 (β-tubulin II) were unchanged between the two mouse genotypes (Fig. 2*D*). There were no differences

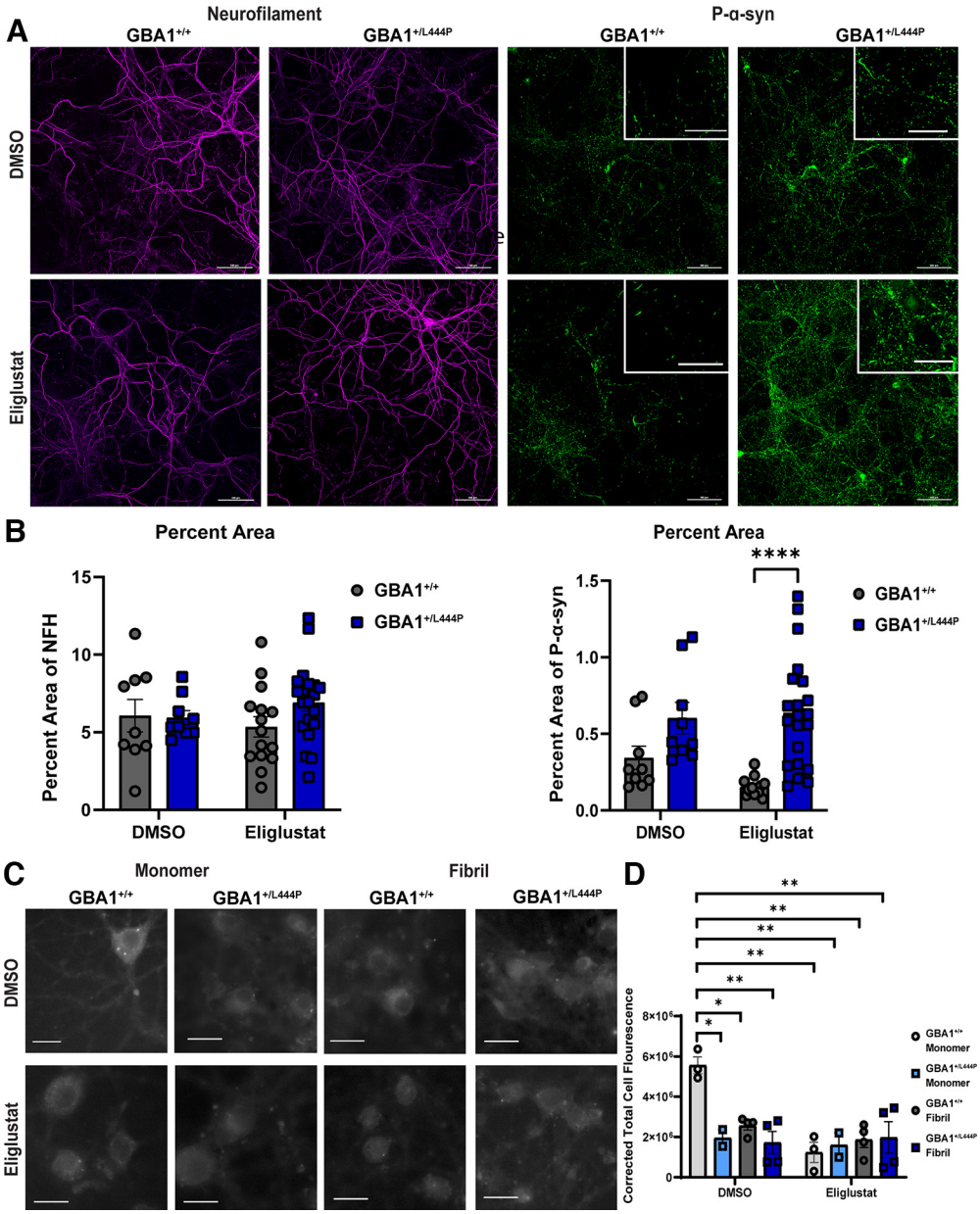

Figure 1. Primary hippocampal neurons from GBA1$^{+/L444P}$ mice show increased α-syn inclusions 14 d after exposure to fibrils and eliglustat, and reduced lysosome activity compared with GBA1$^{+/+}$ mice. ***A***, Representative images of neurofilament-H (magenta, left) and p-α-syn (green, right) in hippocampal primary cultures at DIV21. There were also no differences at DIV14 (Extended Data Fig. 1-1). Top row of panels shows neurons treated with equivalent volumes of DMSO as eliglustat (100 nM, bottom row of panels). GlcCer levels were reduced with 100 nM of eliglustat treatment (Extended Data Fig. 1-2). Scale bars: 100 µm; zoom, 50 µm. ***B***, Quantification of the percent area of NF (left; nested two-way ANOVA; Interaction: Time × genotype: $F_{(1,49)} = 1.365$, $p = 0.2484$, Drug treatment: $F_{(1,49)} = 0.03061$, $p = 0.8618$, Genotype: $F_{(1,49)} = 1.004$, $p = 0.3212$) and p-α-syn (right, nested two-way ANOVA; Time × genotype: $F_{(1,48)} = 1.838$, $p = 0.1815$, Drug treatment: $F_{(1,48)} = 0.8887$, $p = 0.3506$, Genotype: $F_{(1,48)} = 20.29$, $^{****}p < 0.0001$, $N = 9$ for GBA1$^{+/+}$ and GBA1$^{+/L444P}$ DMSO-treated neuron groups, $N = 15$ GBA1$^{+/+}$ eliglustat-treated neurons, $N = 20$ GBA1$^{+/L444P}$ eliglustat-treated neurons). One GBA1$^{+/+}$ DMSO and one GBA1$^{+/L444P}$ DMSO outlier were removed for both NF and p-α-syn analysis based on Grubbs' test. Internalization of fibrils or α-syn expression was not altered by eliglustat treatment (Extended Data Figs. 1-3, 1-4). α-Syn expression was not changed at DIV7 or DIV21 (Extended Data Fig. 1-4). ***C***, Representative images for DQ-BSA assay showing DQ Red BSA (visualized in black and white). Top row of panels shows neurons treated with equivalent volumes of DMSO as eliglustat (100 nM, bottom row of panels) between GBA1$^{+/+}$ and GBA1$^{+/L444P}$ primary hippocampal neurons. ***D***, Quantification of background corrected total cell fluorescence (three-way ANOVA; interaction: $F_{(1,18)} = 3.621$, $p = 0.0732$, Drug treatment × α-syn treatment: $F_{(1,18)} = 7.092$, $^{*}p = 0.0158$, Drug treatment × genotype: $F_{(1,18)} = 9.580$, $^{**}p = 0.0062$, α-syn treatment × genotype: $F_{(1,18)} = 2.512$, $p = 0.1304$, Drug treatment: $F_{(1,18)} = 10.41$, $^{**}p = 0.0047$, α-syn treatment: $F_{(1,18)} = 1.966$, $p = 0.1778$, Genotype: $F_{(1,18)} = 6.234$, $^{*}p = 0.0225$; $N = 3$ for GBA1$^{+/+}$ monomer DMSO and eliglustat-treated neuron groups, $N = 2$ for GBA1$^{+/L444P}$ monomer DMSO and eliglustat-treated neuron groups, $N = 4$ for GBA1$^{+/+}$ and GBA1$^{+/L444P}$ fibril DMSO and eliglustat-treated neurons groups). Eliglustat increased CatB activity only in GBA1$^{+/L444P}$ hippocampal neurons (Extended Data Fig. 1-5). For all graphs, error bars indicate SEM. Scale bar, 100 µm. $^{*}p < 0.05$. $^{**}p < 0.01$. $^{***}p < 0.001$. $^{****}p < 0.0001$.

between GBA1$^{+/L444P}$ mice and GBA1$^{+/+}$ mice in levels of synaptic vesicle SNARE proteins, VAMP2, syntaxin1a, or SNAP-25 (Fig. 2*B*,*E*). Overall, these data show a selective reduction in Triton X-100-soluble p-α-syn and vGLUT1 in GBA1$^{+/L444P}$ without changes in other neuronal or synaptic proteins.

Behavioral tests were also performed in the GBA1$^{+/L444P}$ mice to determine performance in motor activity and associative learning. During the open field test, which evaluates general motor behavior, GBA1$^{+/L444P}$ mice showed no statistical differences in the average velocity, total distance traveled, or the time

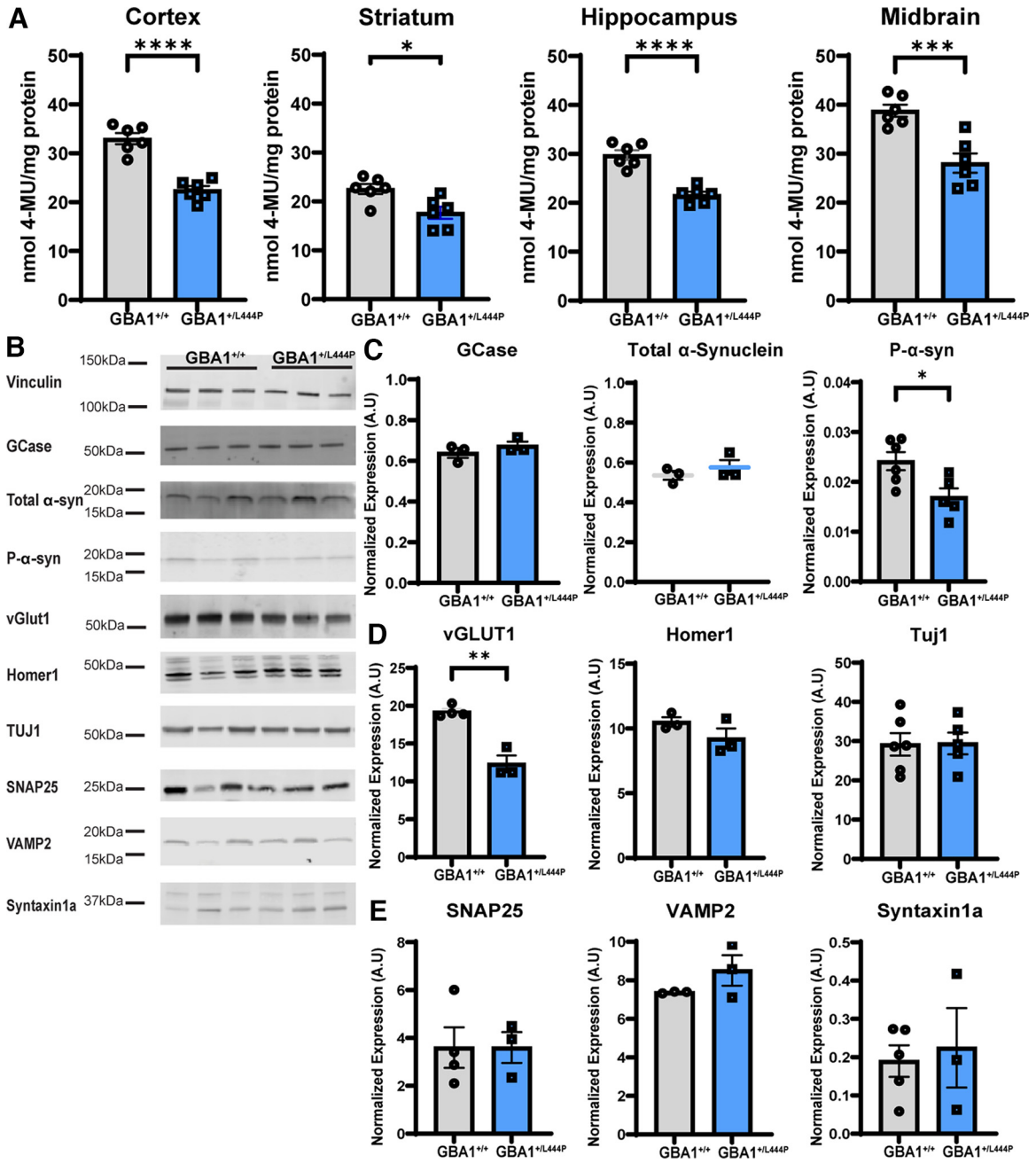

Figure 2. Brain homogenates from GBA1$^{+/L444P}$ mice showed reduced GCase activity and selective reduction of vGLUT1 compared with GBA1$^{+/+}$ mice. ***A***, GCase activity assay to evaluate enzymatic activity of GCase in 2-month-old GBA1$^{+/L444P}$ mice in the cortex (independent *t* test: $t_{(10)} = 7.406$, $^{****}p < 0.0001$), striatum ($t_{(10)} = 3.023$, $^{*}p = 0.0128$), hippocampus ($t_{(10)} = 6.870$, $^{****}p < 0.0001$), and the midbrain ($t_{(10)} = 4.593$; $^{***}p < 0.0010$) expressed as nM 4-MU/mg protein. $N = 6$ for all groups. ***B***, Representative immunoblot analyses of hippocampal brain lysates for GCase, endogenous total α-syn, p-α-syn, Homer1, TUJ1, SNAP25, VAMP2, and syntaxin-1 expression. ***C***, Quantitation of immunoblots; vinculin was used as the loading control to normalize expression. Independent *t* test for GCase ($t_{(4)} = 1.093$, $p = 0.3360$, $N = 3$ for both groups, one GBA1$^{+/+}$ outlier removed) and Mann–Whitney *U* test for endogenous total α-syn ($W = 4$, $p = 0.9999$, $N = 3$ for both groups). An independent *t* test was used for p-α-syn ($t_{(9)} = 2.808$; $^{*}p = 0.0205$, $N = 6$ GBA1$^{+/+}$ and $N = 5$ GBA1$^{+/L444P}$). ***D***, Analysis of vGLUT1 (independent *t* test: $t_{(5)} = 6.686$; $^{**}p = 0.0011$, $N = 4$ GBA1$^{+/+}$ and $N = 3$ GBA1$^{+/L444P}$, one GBA1$^{+/+}$ outlier removed based on Grubbs' test), Homer1 ($t_{(4)} = 1.481$; $p = 0.2127$, $N = 3$ both groups), and TUJ1 ($t_{(9)} = 0.05656$, $p = 0.9561$, $N = 6$ GBA1$^{+/+}$ and $N = 5$ GBA1$^{+/L444P}$) expression. ***E***, Analysis of SNAP25 (independent *t* test: $t_{(5)} = 0005117$, $p = 0.9996$, $N = 4$ GBA1$^{+/+}$ and $N = 3$ GBA1$^{+/L444P}$), VAMP2 ($t_{(4)} = 1.433$, $p = 0.2251$, $N = 3$ in both groups, one GBA1$^{+/+}$ outlier removed), and syntaxin-1a ($t_{(6)} = 0.3713$, $p = 0.7232$, $N = 5$ GBA1$^{+/+}$ and $N = 3$ GBA1$^{+/L444P}$) expression. All immunoblots were run with 3-6 individual mice. For all graphs, error bars indicate SEM. The total synuclein data failed the test for normality and graphed as a scatter plot without a bar using a Mann–Whitney test. $^{*}p < 0.05$. $^{**}p < 0.01$. $^{***}p < 0.001$. $^{****}p < 0.0001$.

spent in the center (Fig. 3*A*). The pole test is used to test basal ganglia motor activity and slowness of movement reflected as increased time to descend pole, in models of PD (Hernandez et al., 2021). GBA1$^{+/L444P}$ mice showed a faster total descent time compared with GBA1$^{+/+}$ mice (Fig. 3*B*, left), but there was no difference in turn-around time or the time descending the pole (Fig. 3*B*, middle and right). Last, fear conditioning was performed to measure associative learning, previously shown to be impaired in mice with fibril-induced inclusions (Stoyka et al., 2020, 2021). During the training phase, both groups of mice showed increased freezing over time in response to a tone paired with a shock with ~73.6% and 73.8% time freezing after foot shock for GBA1$^{+/+}$ and GBA1$^{+/L444P}$ mice, respectively (Fig.

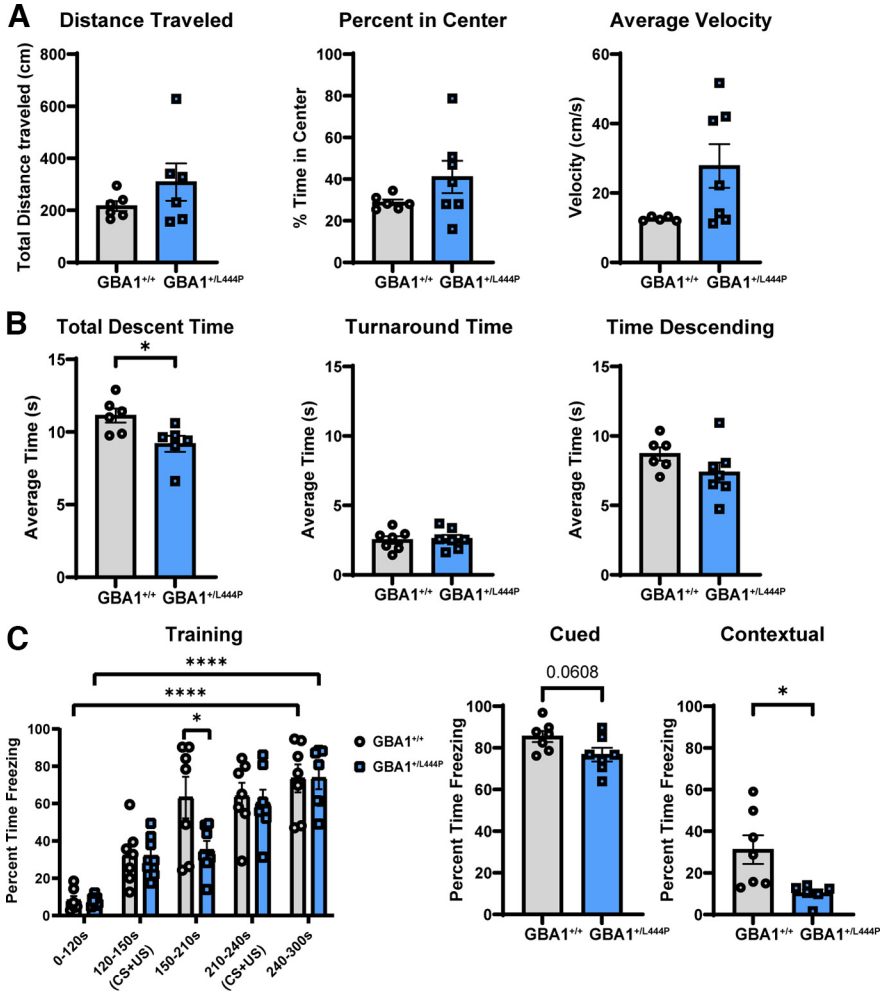

Figure 3. Behavioral analysis of 3-month-old GBA1$^{+/L444P}$ mice compared with GBA1$^{+/+}$ mice. ***A***, Open field test analysis evaluating average velocity (independent *t* test: 2 GBA1$^{+/+}$ outliers removed; $t_{(10)} = 2.002$; $p = 0.0732$, $N = 6$ for both groups), percent in the center (one GBA1$^{+/+}$ outlier removed; $t_{(11)} = 1.436$, $p = 0.1790$, $N = 6$ GBA1$^{+/+}$ $N = 7$ GBA1$^{+/L444P}$), and distance traveled (one GBA1$^{+/+}$ and GBA1$^{+/L444P}$ outlier removed; $t_{(10)} = 1.243$, $p = 0.2424$, $N = 5$ GBA1$^{+/+}$ $N = 7$ GBA1$^{+/L444P}$). ***B***, Pole test evaluated total descent time (one GBA1$^{+/+}$ and GBA1$^{+/L444P}$ outlier removed: $t_{(10)} = 2.638$, $^*p = 0.0248$, $N = 6$ for both groups), turnaround time ($t_{(12)} = 0.2243$, $p = 0.8263$, $N = 7$ for both groups), and time descending (one GBA1$^{+/+}$ outlier removed; $t_{(11)} = 1.467$; $p = 0.1704$, $N = 6$ GBA1$^{+/+}$ $N = 7$ GBA1$^{+/L444P}$). ***C***, Fear conditioning analysis evaluated percent time spent freezing in training (repeated-measures two-way ANOVA: time: $F_{(4,48)} = 49.13$, $^{****}p < 0.0001$, genotype: $F_{(1,12)} = 1.106$, $p = 0.3136$, time × genotype: $F_{(4,48)} = 2.751$, $^*p = 0.0386$), cued fear conditioning (independent *t* test: $t_{(12)} = 2.069$, $p = 0.0608$), and contextual fear conditioning ($t_{(11)} = 2.720$, $^*p = 0.0199$, one GBA1$^{+/L444P}$ outlier removed). $N = 7$ for both groups. For all graphs, error bars indicate SEM. $^*p < 0.05$. $^{***}p < 0.001$. $^{****}p < 0.0001$.

3*C*, left). The next day, memory and fear responses were tested by measuring the time spent freezing. In cued fear conditioning, mice were placed in a novel environment and exposed to the CS used for training. GBA1$^{+/L444P}$ mice and GBA1$^{+/+}$ mice exhibited no statistical difference in the percentage of time spent freezing ($t_{(12)} = 2.069$; $p = 0.0608$) (Fig. 3*C*, middle). In contextual fear conditioning, mice were placed in the same environment as the training without the presence of the tone. GBA1$^{+/L444P}$ mice froze less than GBA1$^{+/+}$ mice (Fig. 3*C*, right). Despite variability among GBA1$^{+/L444P}$ mice, no weight or percent time freezing differences between sex were observed (data not shown). Thus, the GBA1$^{+/L444P}$ mice showed impairment in contextual fear memory.

Levels of GlcCers and GlcSph in GBA1$^{+/L444P}$ mice and GBA1$^{+/+}$ mice at different ages

Defects in sphingolipid metabolism because of reduced GCase activity are prevalent in Gaucher's disease and have been implicated in PD (Mazzulli et al., 2011; Belmatoug et al., 2017; Taguchi et al., 2017). Thus, we evaluated the accumulation of GlcCer and GlcSph in the forebrain in 3-, 6-, 9-, and 12-month-old GBA1$^{+/+}$ mice and GBA1$^{+/L444P}$ mice. In GBA1$^{+/+}$ mice, levels of GlcSph were significantly increased in 12-month-old mice compared with younger mice. GlcSph levels were significantly higher in the brains of GBA1$^{+/L444P}$ mice compared with GBA1$^{+/+}$ mice by 6 months of age. GlcSph levels increased with age in the GBA1$^{+/L444P}$ mice as well (Fig. 4*A*). In contrast, GlcCer levels remained unchanged between GBA1$^{+/+}$ and GBA1$^{+/L444P}$ mice (Fig. 4*B*). To evaluate whether different acyl chain length structural variants of GlcCer were altered with age and the presence of the GBA1$^{+/L444P}$ mutation, we evaluated four isoforms of GlcCer. GlcCer18:0 decreased with age in GBA1$^{+/+}$ mice but reached a plateau at 9 months of age (Extended Data Fig. 4-1*A*). However, there were no statistical differences between the GlcCer20:0, GlcCer22:0, and GlcCer24:1 isoform in either GBA1$^{+/+}$ or GBA1$^{+/L444P}$ mice (Extended Data Fig. 4-1*B-D*).

Recent studies have evaluated the effective use of lipid substrates in patient plasma as a potential biomarker of disease. Plasma GlcSph levels correlate with disease burden in Gaucher's disease (Murugesan et al., 2016). Moreover, a recent study implemented the usefulness of GlcSph in GBA1-PD as a biomarker of disease (Surface et al., 2022). Thus, we evaluated the accumulation of lipids in the plasma of GBA1$^{+/+}$ and GBA1$^{+/L444P}$ mice at the time of death. Similar to findings in brain homogenates, GlcSph was increased in the plasma of GBA1$^{+/L444P}$ mice compared with GBA1$^{+/+}$, while GlcCer remained unchanged (Fig. 4*C*,*D*).

Fibril-induced α-syn inclusions in GBA1$^{+/L444P}$ mice compared with GBA1$^{+/+}$ mice

GBA1$^{+/+}$ and GBA1$^{+/L444P}$ mice were injected bilaterally in the dorsolateral striatum with fibrils or monomer to induce α-syn inclusion formation. Starting 1 week after injections until death, mice were fed chow containing venglustat or control chow to determine whether inhibiting GCS, and consequently reducing the synthesis of glycosphingolipids, reduces formation of α-syn inclusions. Ten months after injection, mice were perfused, and IF was performed on fixed brain sections for p-α-syn-positive inclusions. The dmPFC, hippocampus, and SNc were analyzed as previously described (Stoyka et al., 2020, 2021). Mice injected with monomer showed no p-α-syn inclusions, regardless of GBA1L444P expression as previously shown in our publications (Froula et al., 2019; Stoyka et al., 2020). Abundant inclusions

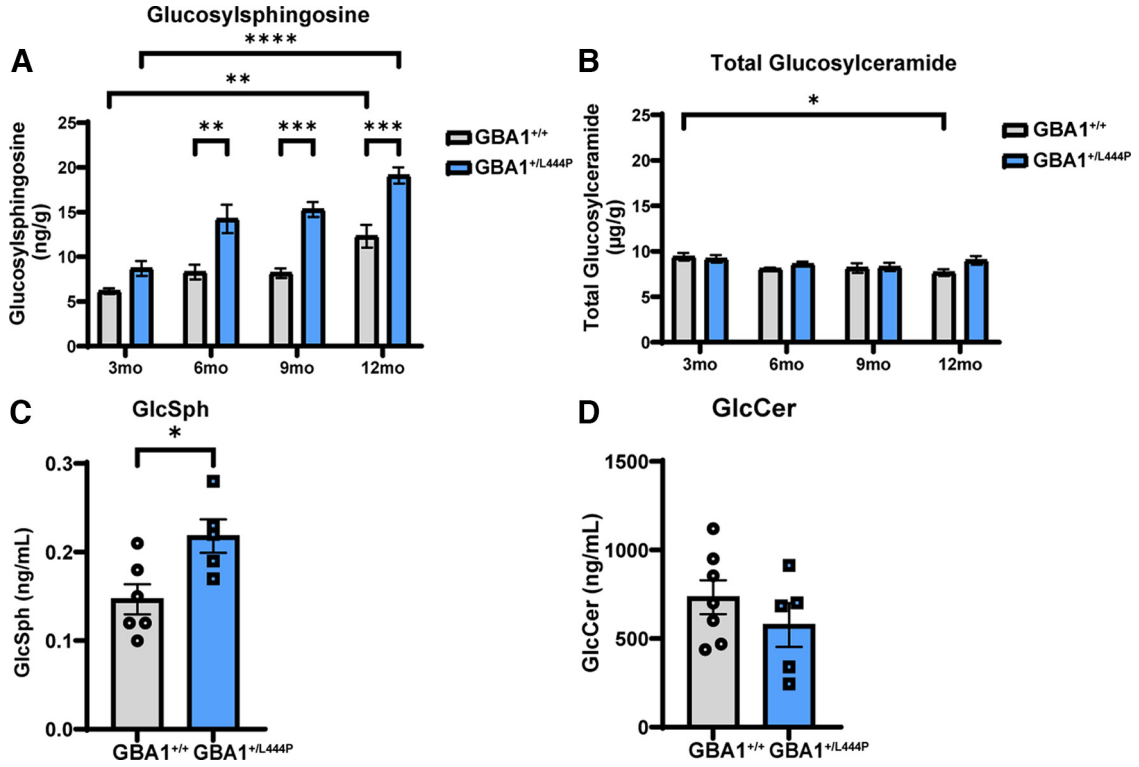

Figure 4. Lipid analysis in GBA1$^{+/+}$ and GBA1$^{+/L444P}$ mice. GBA1$^{+/+}$ and GBA1$^{+/L444P}$ mice forebrains underwent mass spectrometry for lipid quantification for (***A***) GlcSph (two-way ANOVA; Interaction: $F_{(3,50)} = 2.270$, $p = 0.0918$, Age: $F_{(3,50)} = 23.54$, ****$p < 0.0001$, and Genotype: $F_{(1,50)} = 64.23$, ****$p < 0.0001$) and (***B***) total GlcCer (Interaction: $F_{(3,50)} = 1.454$, $p = 0.2384$, Age: $F_{(3,50)} = 3.340$, *$p = 0.0265$, Genotype: $F_{(1,50)} = 2.493$, $p = 0.1206$) at 3, 6, 9, and 12 months. ***C***, Mice plasma was collected and underwent mass spectrometry for lipid quantification for ***C***. GlcSph (independent *t* test, $t_{(9)} = 2.810$, *$p = 0.0204$, $N = 6$ for GBA1$^{+/+}$, and $N = 5$ GBA1$^{+/L444P}$) and (***D***) GlcCer ($t_{(10)} = 1.015$, $p = 0.3338$, $N = 7$ for GBA1$^{+/+}$ and $N = 5$ GBA1$^{+/L444P}$). Only GlcCer d18:1_18:0 isoform was reduced in aged GBA1$^{+/+}$ mice with no changes between GBA1L444P expression (Extended Data Fig. 4-1). For all graphs, error bars indicate SEM. *$p < 0.05$. **$p < 0.01$. ***$p < 0.001$. ****$p < 0.0001$.

were seen in dmPFC, SNc, and the hippocampus in the fibril-injected GBA1$^{+/+}$ mice and GBA1$^{+/L444P}$ mice. There were no significant differences in the pathologic p-α-syn load in the dmPFC between genotypes in mice that received control chow (Fig. 5*A*,*B*). In the hippocampus, GBA1$^{+/L444P}$ mice had significantly more p-α-syn inclusions than GBA1$^{+/+}$ mice in the control treatment group in the dentate gyrus and CA1 pyramidal cell layer (Fig. 5*C*,*D*). Finally, there were no significant differences or patterns in pathologic load between GBA1L444P expression and treatment conditions in the SNc (Fig. 5*E*,*F*), basolateral amygdala, and entorhinal cortex (Extended Data Fig. 5-1).

To determine whether inhibiting GCS prevented α-syn inclusion formation, mice were provided with chow with venglustat or control chow. To ensure the biological activity of venglustat treatment, plasma was acquired from the mice groups at the time of death, and mass spectrometry was performed to measure GlcCer concentrations. Compared with control mice, GlcCer was significantly reduced in all venglustat-treated mice (Extended Data Fig. 5-2*A*). Mice administered venglustat showed significantly reduced plasma levels of GlcCer, confirming the efficacy of the compound. However, GBA1$^{+/+}$ mice fed control chow did not show a difference in abundance of α-syn inclusions between GBA1$^{+/+}$ mice treated with venglustat in any of the evaluated brain regions (Fig. 5). GBA1$^{+/L444P}$ mice treated with venglustat did show significantly fewer inclusions in the mPFC than both GBA1$^{+/+}$ mice and GBA1$^{+/L444P}$ mice that were not treated with venglustat (Fig. 5*A*,*B*). This difference was not because of cell death as there were no changes in the quantity of NeuN^{+} cells between any groups (Extended Data Fig. 5-3). Although underpowered, treatment with venglustat did not reduce the abundance of α-syn inclusions in the hippocampus (Fig. 5*C*,*D*). There were also no differences in α-syn inclusions in the SNc (Fig. 5*E*,*F*). Differences in pathology were not a result of differences in expression levels of endogenous α-syn (Extended Data Fig. 5-4).

Neuroinflammation in GBA1$^{+/L444P}$ mice compared with GBA1$^{+/+}$ mice

Expression of the GBA1L444P mutation causes systemic inflammation in addition to enhanced neuroinflammation clinically and in this mouse model (Mizukami et al., 2002; Rocha et al., 2015; Mus et al., 2019; Brunialti et al., 2021; Williams et al., 2021). Thus, 10 months after monomer or fibril injection, hippocampal brain sections were stained for MHCII and IgG to investigate inflammation. Despite the increased accumulation of pathologic α-syn in fibril-injected GBA1$^{+/L444P}$ mice, the granule cell layer of the dentate gyrus showed no differences between IgG and MHCII abundance across all groups (Extended Data Fig. 5-5).

Fibril-induced loss of TH-positive dopaminergic neurons in the SNc in GBA1$^{+/+}$ mice and GBA1$^{+/L444P}$ mice

Fibril-induced formation of α-syn inclusions leads to the death of dopamine neurons in the SNc (Luk et al., 2012; Froula et al., 2019; Stoyka et al., 2021). To test whether GBA1$^{+/L444P}$ mice show enhanced dopaminergic loss, IHC and unbiased stereology were performed by targeting Tyrosine Hydroxylase (TH) to quantify SNc dopamine neurons. Both GBA1$^{+/+}$ mice and GBA1$^{+/L444P}$ mice injected with fibrils had an ~50% reduction of dopaminergic neurons in the SNc compared with GBA1$^{+/+}$

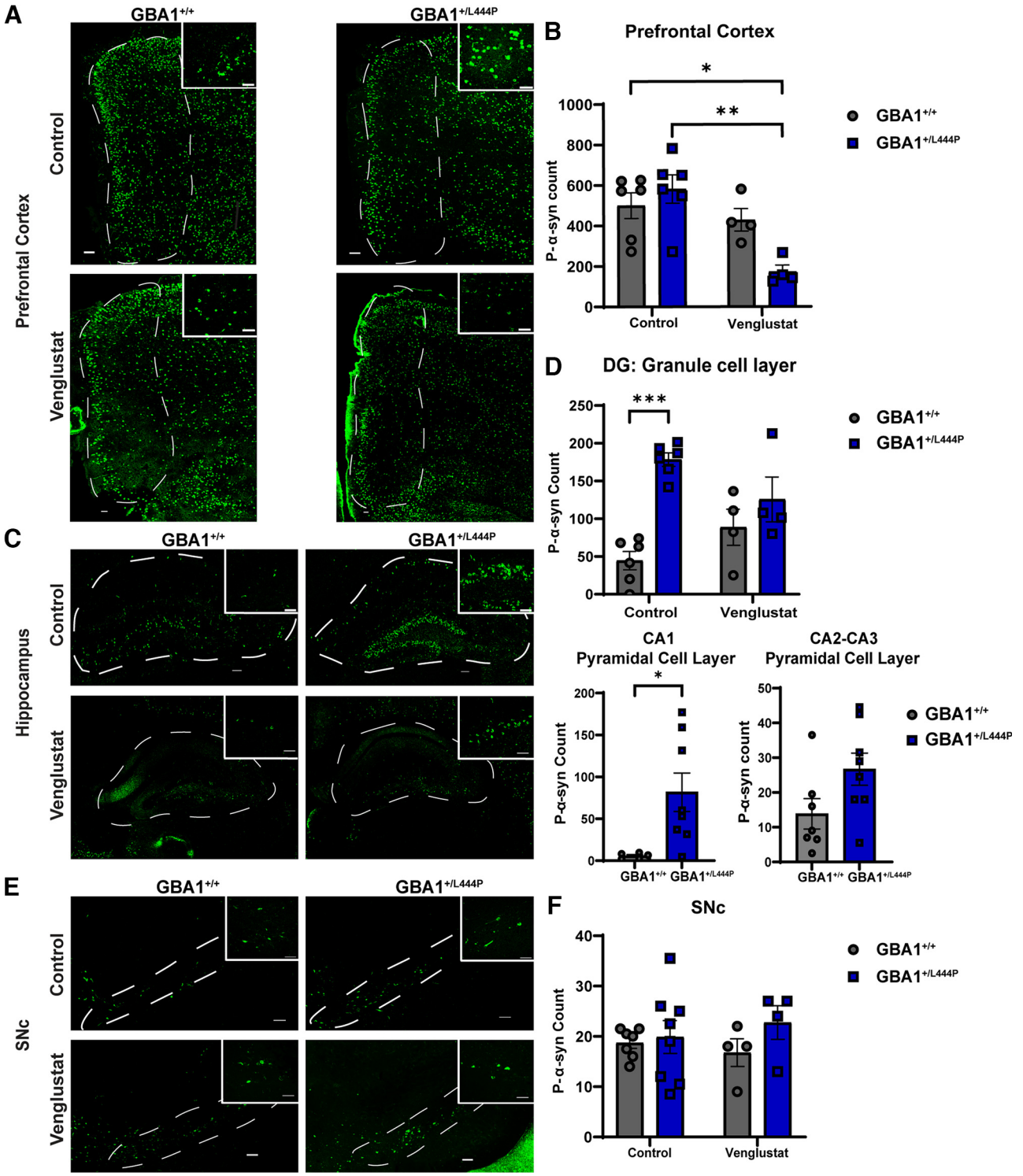

Figure 5. p-α-syn pathology burden is increased in the hippocampal formation. ***A***, Ten months after bilateral striatal injections, IF for p-α-syn was performed. Representative images of GBA1$^{+/+}$ and GBA1$^{+/L444P}$ fibril-injected mice fed control or venglustat chow of the dmPFC were captured using confocal microscopy. Venglustat chow reduced GlcCer (Extended Data Fig. 5-2). Scale bars: 100 μm; zoom, 50 μm. ***B***, Quantification of p-α-syn in the dmPFC ($N = 6$ for both control chow groups, $N = 4$ for venglustat chow groups). Two-way ANOVA: Interaction: $F_{(1,16)} = 6.890$, $^{*}p = 0.0184$, Drug treatment: $F_{(1,16)} = 13.95$, $^{**}p = 0.0018$, Genotype: $F_{(1,16)} = 1.842$, $p = 0.1936$. Error bars indicate SEM. Changes in p-α-syn inclusions in the PFC was not because of changes in cell quantity (Extended Data Fig. 5-3). ***C***, Representative images of GBA1$^{+/+}$ and GBA1$^{+/L444P}$ fibril-injected mice fed control or venglustat chow of the hippocampus were captured using confocal microscopy. Scale bars: 100 μm; zoomed, 50 μm. ***D***, Quantification of p-α-syn in the granule cell layer of the dentate gyrus area of the hippocampus ($N = 6$ for both control chow groups, $N = 4$ for venglustat chow groups, two outliers removed (one GBA1$^{+/+}$ and one GBA1$^{+/L444P}$). Interaction: $F_{(1,16)} = 7.484$, $^{*}p = 0.0147$, Drug treatment: $F_{(1,16)} = 0.05575$, $p = 0.8163$, Genotype: $F_{(1,16)} = 23.18$, $^{***}p = 0.0002$. Quantification of CA1-CA3 pyramidal cell layer with control chow ($N = 7$ GBA1$^{+/+}$ and $N = 8$ GBA1$^{+/L444P}$: *t* test: CA1 pyramidal cell layer: $t_{(11)} = 2.580$; $^{*}p = 0.0256$, CA2-CA3 pyramidal cell layer: $t_{(13)} = 1.997$; $p = 0.0672$). Error bars indicate SEM. ***E***, Representative images of GBA1$^{+/+}$ and GBA1$^{+/L444P}$ fibril-injected mice fed control or venglustat chow of the SNc were captured using confocal microscopy. Scale bars: 100 μm; zoom, 50 μm. ***F***, Quantification of p-α-syn in the SNc ($N = 7$ for GBA1$^{+/+}$ and $N = 8$ for GBA1$^{+/L444P}$ control chow groups, $N = 4$ for GBA1$^{+/+}$ and GBA1$^{+/L444P}$ venglustat chow groups).

mice injected with α-syn monomer (Fig. 6*A*,*C*) as previously shown (Froula et al., 2019; Stoyka et al., 2020, 2021). Similarly, GBA1$^{+/L444P}$ fibril-injected mice treated with venglustat showed a 50% decrease in TH^{+} neurons compared with GBA1$^{+/+}$ monomer injected mice fed venglustat. However, no differences between GBA1L444P expression, nor between venglustat and control chow, were observed. Thus, venglustat did not protect SNc neurons from toxicity caused by fibril-induced α-syn inclusions (Fig. 6*B*,*C*).

Behavioral analyses in fibril-injected GBA1$^{+/L444P}$ mice compared with GBA1$^{+/+}$ mice, with and without venglustat

Our laboratory previously showed that fibril-induced α-syn inclusions cause motor and nonmotor phenotypes (Froula et al., 2019; Stoyka et al., 2020). We evaluated how motor and nonmotor phenotypes are impacted in GBA1$^{+/L444P}$ mice injected with fibrils and the effect of venglustat treatment. A Kaplan–Meier survival curve showed that GBA1$^{+/L444P}$ monomer mice provided with venglustat chow died statistically significantly more often than the GBA1$^{+/+}$ or GBA1$^{+/L444P}$ monomer mice or the GBA1$^{+/+}$ monomer-injected mice fed venglustat chow (Fig. 7*A*, left). However, when comparing fibril-injected mice, there were no statistical differences between any groups (Fig. 7*A*, right).

To evaluate motor behavior, an open field test was performed and showed no statistical differences in any groups for total distance traveled, or average velocities. In addition, there were no differences among groups with respect to percent time in the center. Although the venglustat-treated group showed less time in the center (Drug treatment: $F_{(1,70)} = 5.160$, $^{*}p = 0.0262$), the Tukey's *post hoc* test detected no statistical differences between groups (Fig. 7*B*). For the pole test, GBA1$^{+/+}$ mice injected with fibrils and GBA1$^{+/L444P}$ mice injected with fibrils and fed venglustat chow spent increased time turning around on the pole compared with GBA1$^{+/+}$ mice injected with monomer, indicative of reduced motor function consistent with previous literature (Fig. 7*C*, left) (Froula et al., 2019).

Last, to test for associative learning, fear conditioning was used as described in Figure 3. During the training phase, all mice fed control chow displayed an increase in the percent of time spent freezing ranging from 63% to 78%. (Fig. 7*D*, left). However, in venglustat-treated mice, only GBA1$^{+/+}$ mice injected with monomeric α-syn displayed an increase in freezing of ~82% (Fig. 7*D*, right). No other differences between control and venglustat-fed mice were observed (data not shown). The next day, mice were assessed for memory by going through cued and contextual fear conditioning as described in Figure 2. For contextual fear conditioning, mice freezing behavior was examined during the first minute. However, all mice groups displayed equal percent time freezing from 52% to 75% across venglustat-treated groups and 56%-69% in control-treated mice groups (Fig. 7*E*, left). In cued fear conditioning, only GBA1$^{+/+}$ fibril-injected mice fed control chow reduced by 12.43% in freezing behavior compared with GBA1$^{+/+}$ monomer-injected mice fed control chow. There were no differences among any other groups (Fig. 7*E*, left). Given the variance and multiple groups in these analyses, we performed a power analysis. Given the effect size 0.18, with an $\alpha = 0.05$, power of 80%, an $N = 18$ per group would be needed to achieve statistically significant differences.

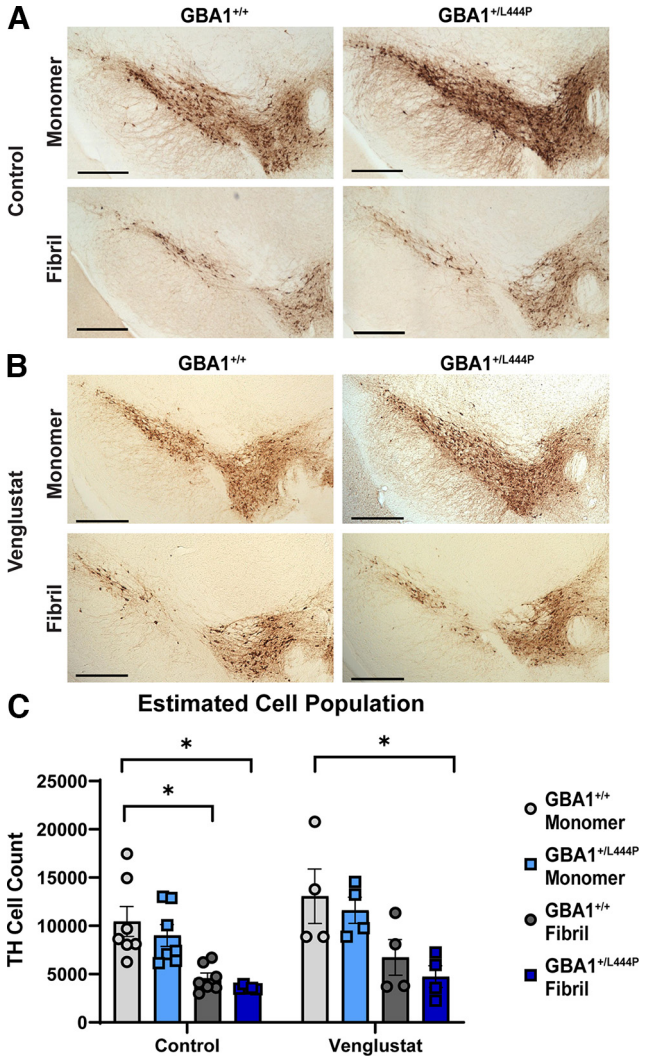

Figure 6. Quantification of dopaminergic neuron cell death. IHC for TH was performed in GBA1$^{+/+}$ and GBA1$^{+/L444P}$ mice at 10 months after injection, and the SNc was analyzed for dopaminergic cell death using unbiased stereology. ***A***, Representative images of monomer and fibril-injected GBA1$^{+/+}$ and GBA1$^{+/L444P}$ mice fed control chow ($N = 7$ for all groups). ***B***, Representative images of monomer and fibril-injected GBA1$^{+/+}$ and GBA1$^{+/L444P}$ mice fed venglustat chow ($N = 4$ for all groups). ***C***, Unbiased stereology was used to estimate TH^{+} cell count (three-way ANOVA: Interaction: $F_{(1,34)} = 0.06097$, $p = 0.8065$, Drug treatment × α-syn treatment: $F_{(1,34)} = 0.2240$, $p = 0.6390$, Drug treatment × genotype: $F_{(1,34)} = 0.06160$, $p = 0.8055$, α-syn treatment × genotype: $F_{(1,34)} = 0.0002467$, $p = 0.9876$, Drug treatment: $F_{(1,34)} = 4.451$, $^{*}p = 0.0423$, α-syn treatment: $F_{(1,34)} = 36.68$, $^{****}p < 0.0001$, Genotype: $F_{(1,34)} = 2.122$, $p = 0.1544$). Error bars indicate SEM. Scale bar, 200 μm. $^{*}p < 0.05$.

Discussion

Heterozygosity for the GBA1L444P mutation increases the risk of developing PDD (Cilia et al., 2016). However, the mechanisms by which GBA1L444P could increase cognitive deficits are relatively unclear. Here, we show that levels of GlcSph, but not levels of GlcCer, are increased in GBA1$^{+/L444P}$ and aged GBA1$^{+/+}$ mice. Since age may be the primary risk factor for the development

←

Two-way ANOVA: Interaction: $F_{(1,19)} = 0.6662$, $p = 0.4245$, Drug treatment: $F_{(1,19)} = 0.02359$, $p = 0.8795$, Genotype: $F_{(1,19)} = 1.459$, $p = 0.2420$. The entorhinal cortex and amygdala showed no changes in p-α-syn inclusions (Extended Data Fig. 5-1). Total α-syn expression was not changed between any brain regions (Extended Data Fig. 5-4). There were no changes in MHCII or IgG in the hippocampus (Extended Data Fig. 5-5). For all graphs, error bars indicate SEM. $^{*}p < 0.05$. $^{**}p < 0.01$. $^{***}p < 0.001$.

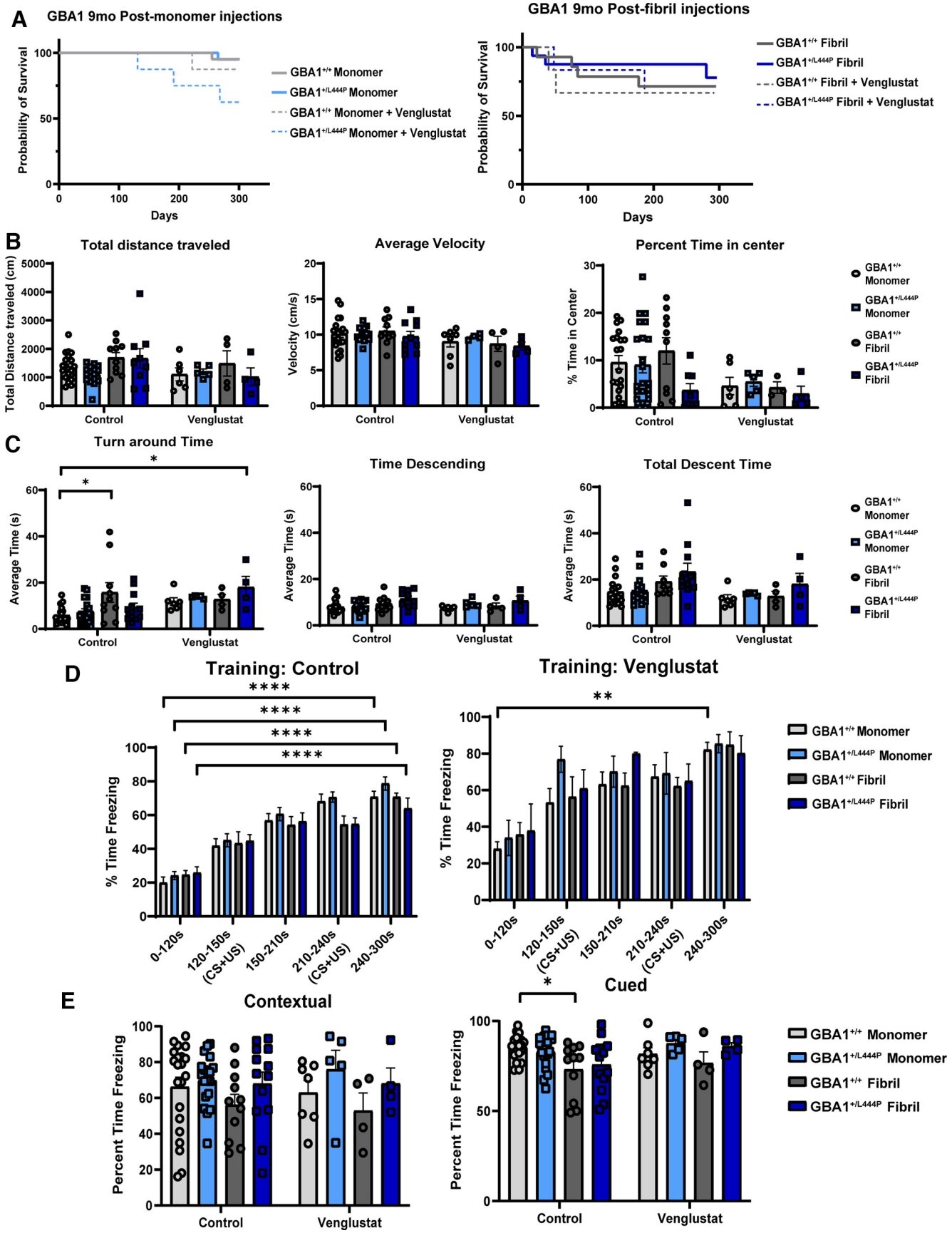

Figure 7. Behavioral analyses of monomer and fibril-injected mice fed venglustat or control chow. GBA1$^{+/+}$ and GBA1$^{+/L444P}$ mice underwent behavioral test to evaluate motor and cognitive function 7 months after fibril or monomer injection and venglustat or control treatment. ***A***, Quantification of mouse survival using a Kaplan–Meier survival curve (log-rank (Mantel–Cox) test: after monomer injection: χ^2 (3, $N = 57$) = 8.722, *$p = 0.0332$, after fibril injection: χ^2 (3, $N = 42$) = 0.6481, $p = 0.8853$). ***B***, Open

of PD, these data indicate a potential pathologic role for increased levels of GlcSph in the brain (Taguchi et al., 2017). Our data also support that plasma GlcSph is relevant biomarker for GBA1-PD. Furthermore, neurons from GBA1$^{+/L444P}$ mice show reduced hippocampal lysosome function, and expression of vGLUT1, without changes in other synaptic proteins. Thus, GBA1$^{+/L444P}$ expression alone may increase the susceptibility of neurons by impacting lysosome and synapse biology; however, further investigation is required. GBA1$^{+/L444P}$ mice show defects in contextual fear conditioning which depends on hippocampal function as well as increased pathologic α-syn, compared GBA1$^{+/+}$ mice. These findings suggest that GBA1L444P mutations may selectively affect neurons in limbic brain areas which could have implications for cognitive decline in GBA1-PD.

Clinically, PDD, DLB, and GBA1-PD patients demonstrate similar cognitive symptoms, involving deficits in hippocampal-dependent tasks, including short-term memory, visual-spatial function, and executive function (Alcalay et al., 2012; Zokaei et al., 2014; Gomperts, 2016; O'Shea et al., 2016; Leocadi et al., 2022; Vieira and Schapira, 2022). The GBA1$^{+/L444P}$ mutation is considered a severe neuronopathic mutation as it is correlated to neurologic defects, including cognitive decline (Szwedo et al., 2022). We demonstrate that the GBA1$^{+/L444P}$ mutation alone, even in the absence of fibril-induced inclusions, leads to memory deficits. Thus, the preclinical model supports findings that neuronopathic *GBA1* mutations may sensitize individuals to cognitive impairments. GBA1$^{+/L444P}$ mice also show reduced hippocampal expression of vGLUT1, but no changes in expression of synaptic components of the SNARE complex. Given how vGLUT1 is predominantly expressed in cortical and hippocampal regions (Wojcik et al., 2004), this reduction may underlie contextual associative memory deficits seen concurrently.

Given our findings that GCase activity is reduced in the hippocampus, cortex, and midbrain, we would expect an increase in aggregate burden in these regions as indicated in previous literature (Cullen et al., 2011; Mazzulli et al., 2011; Sardi et al., 2011; Henderson et al., 2020; Migdalska-Richards et al., 2020). However, enhanced pathologic α-syn is only observed in the hippocampus, specifically in the granule cell layer of the dentate gyrus and the pyramidal cell layer of the CA1 region. Under physiological conditions, GCase is highly expressed in the hippocampus and entorhinal cortex (Dopeso-Reyes et al., 2018). Interestingly, hippocampal Math2^{+} CA neuronal subpopulations express higher expression of endogenous α-syn and are therefore more susceptible to pathology (Luna et al., 2018). Our laboratory showed that pathologic α-syn localizes to excitatory

←

field test analysis evaluating the total distance traveled (three-way ANOVA: Interaction: $F_{(1,66)} = 1.655$, $p = 0.2028$, Drug treatment × α-syn treatment: $F_{(1,66)} = 1.201$, $p = 0.2771$, Drug treatment × genotype: $F_{(1,66)} = 0.01696$, $p = 0.8968$, α-syn treatment × genotype: $F_{(1,66)} = 0.2655$, $p = 0.6081$, Drug treatment: $F_{(1,66)} = 2.578$, $p = 0.1131$, α-syn treatment: $F_{(1,66)} = 2.965$, $p = 0.0898$, Genotype: $F_{(1,66)} = 1.084$, $p = 0.3016$, Control: Monomer-injected GBA1$^{+/+}$ $N = 20$, Monomer-injected GBA1$^{+/L444P}$ $N = 16$, Fibril-injected GBA1$^{+/+}$ $N = 10$ (one outlier removed), Fibril-injected GBA1$^{+/L444P}$ $N = 9$. Venglustat: Monomer-injected GBA1$^{+/+}$ $N = 6$, Monomer-injected GBA1$^{+/L444P}$ $N = 5$, and Fibril-injected GBA1$^{+/+}$ and GBA1$^{+/L444P}$ $N = 4$), average velocity (Interaction: $F_{(1,66)} = 0.02006$, $p = 0.8878$, Drug treatment × α-syn treatment: $F_{(1,66)} = 0.7082$, $p = 0.4031$, Drug treatment × genotype: $F_{(1,66)} = 0.3206$, $p = 0.5732$, α-syn treatment × genotype: $F_{(1,66)} = 0.6204$, $p = 0.4337$, Drug treatment: $F_{(1,66)} = 5.121$, $^{*}p = 0.0269$, α-syn treatment: $F_{(1,66)} = 0.5298$, $p = 0.4693$, Genotype: $F_{(1,66)} = 0.05453$, $p = 0.8161$, Control: Monomer-injected GBA1$^{+/+}$ $N = 20$, Monomer-injected GBA1$^{+/L444P}$ $N = 16$ (two outliers removed), Fibril-injected GBA1$^{+/+}$ and GBA1$^{+/L444P}$ $N = 10$. Venglustat: Monomer-injected GBA1$^{+/+}$ $N = 7$, Monomer-injected GBA1$^{+/L444P}$ $N = 4$, Fibril-injected GBA1$^{+/+}$ and GBA1$^{+/L444P}$ $N = 4$), and the percent time in the center (Interaction: $F_{(1,70)} = 0.5531$, $p = 0.4596$, Drug treatment × α-syn treatment: $F_{(1,70)} = 0.0002562$, $p = 0.9873$, Drug treatment × genotype: $F_{(1,70)} = 1.246$, $p = 0.2681$, α-syn treatment × genotype: $F_{(1,70)} = 1.774$, $p = 0.1872$, Drug treatment: $F_{(1,70)} = 5.160$, $^{*}p = 0.0262$, α-syn treatment: $F_{(1,70)} = 0.5955$, $p = 0.4429$, Genotype: $F_{(1,70)} = 1.535$, $p = 0.2195$, Control: Monomer-injected GBA1$^{+/+}$ $N = 20$, Monomer-injected GBA1$^{+/L444P}$ $N = 22$ (one outlier removed), Fibril-injected GBA1$^{+/+}$ $N = 10$ (one outlier removed), Fibril-injected GBA1$^{+/L444P}$ $N = 8$ (two outliers removed). Venglustat: Monomer-injected GBA1$^{+/+}$ $N = 6$, Monomer-injected GBA1$^{+/L444P}$ $N = 5$, Fibril-injected GBA1$^{+/+}$ $N = 3$ (one outlier removed), Fibril-injected GBA1$^{+/L444P}$ $N = 4$). ***C***, Mice underwent pole test to evaluate motor deficits by analyzing the time descending (three-way ANOVA: Interaction: $F_{(1,62)} = 0.2636$, $p = 0.6095$, Drug treatment × α-syn treatment: $F_{(1,62)} = 0.4947$, $p = 0.4845$, Drug treatment × genotype: $F_{(1,62)} = 0.3006$, $p = 0.5855$, α-syn treatment × genotype: $F_{(1,62)} = 0.3767$, $p = 0.5416$, Drug treatment: $F_{(1,62)} = 0.2163$, $p = 0.6435$, α-syn treatment: $F_{(1,62)} = 4.483$, $^{*}p = 0.0382$, Genotype: $F_{(1,62)} = 4.874$, $^{*}p = 0.0310$, Control: Monomer-injected GBA1$^{+/+}$ $N = 17$, Monomer-injected GBA1$^{+/L444P}$ N = 15, Fibril-injected GBA1$^{+/+}$ $N = 9$, Fibril-injected GBA1$^{+/L444P}$ $N = 10$. Venglustat: Monomer-injected GBA1$^{+/+}$ $N = 6$, Monomer-injected GBA1$^{+/L444P}$ $N = 5$, Fibril-injected GBA1$^{+/+}$ and GBA1$^{+/L444P}$ $N = 4$), turnaround time (Interaction: $F_{(1,69)} = 2.500$, $p = 0.1184$, Drug treatment × α-syn treatment: $F_{(1,69)} = 0.8307$, $p = 0.3652$, Drug treatment × genotype: $F_{(1,69)} = 2.814$, $p = 0.0980$, α-syn treatment × genotype: $F_{(1,69)} = 0.4537$, $p = 0.5028$, Drug treatment: $F_{(1,69)} = 6.223$, $^{*}p = 0.0150$, α-syn treatment: $F_{(1,69)} = 5.396$, $^{*}p = 0.0231$, Genotype: $F_{(1,69)} = 0.1263$, $p = 0.7234$; Control: Monomer-injected GBA1$^{+/+}$ $N = 18$, Monomer-injected GBA1$^{+/L444P}$ $N = 18$, Fibril-injected GBA1$^{+/+}$ $N = 10$, Fibril-injected GBA1$^{+/L444P}$ $N = 12$. Venglustat: Monomer-injected GBA1$^{+/+}$ $N = 6$, Monomer-injected GBA1$^{+/L444P}$ $N = 5$, Fibril-injected GBA1$^{+/+}$ and GBA1$^{+/L444P}$ $N = 4$), and total descent time (Interaction: $F_{(1,62)} = 0.003431$, $p = 0.9535$, Drug treatment × α-syn treatment: $F_{(1,62)} = 0.8643$, $p = 0.3561$, Drug treatment × genotype: $F_{(1,62)} = 0.09758$, $p = 0.7558$, α-syn treatment × genotype: $F_{(1,62)} = 0.7574$, $p = 0.3875$, Drug treatment: $F_{(1,62)} = 3.983$, $p = 0.0504$, α-syn treatment: $F_{(1,62)} = 4.805$, $^{*}p = 0.0321$, Genotype: $F_{(1,62)} = 2.267$, $p = 0.1372$; Control: Monomer-injected GBA1$^{+/+}$ $N = 17$, Monomer-injected GBA1$^{+/L444P}$ $N = 15$, Fibril-injected GBA1$^{+/+}$ $N = 8$, Fibril-injected GBA1$^{+/L444P}$ $N = 11$. Venglustat: Monomer-injected GBA1$^{+/+}$ $N = 6$, Monomer-injected GBA1$^{+/L444P}$ $N = 5$, Fibril-injected GBA1$^{+/+}$ and GBA1$^{+/L444P}$ $N = 4$). ***D***, Quantification of the training phase of fear conditioning for monomer or fibril-injected GBA1$^{+/+}$ or GBA1$^{+/L444P}$ mice fed control chow (repeated-measures three-way ANOVA: Interaction: $F_{(4240)} = 0.6830$, $p = 0.6044$, Time × α-syn treatment: $F_{(4240)} = 4.425$, $^{**}p = 0.0018$, Time × genotype: $F_{(4240)} = 0.0877$, $p = 0.9862$, α-syn treatment × genotype: $F_{(1,60)} = 0.6170$, $p = 0.4353$, Time: $F_{(4240)} = 120.1$, $^{****}p < 0.0001$, α-syn treatment: $F_{(1,60)} = 2.12$, $p = 0.1506$, Genotype: $F_{(1,60)} = 0.4373$, $p = 0.5110$, GBA1$^{+/+}$ Monomer $N = 21$, GBA1$^{+/L444P}$ Monomer $N = 19$, GBA1$^{+/+}$ fibril $N = 10$, GBA1$^{+/L444P}$ fibril $N = 13$) and venglustat chow (Interaction: $F_{(4,64)} = 0.5828$, $p = 0.6762$, Time × α-syn treatment: $F_{(4,64)} = 0.5808$, $p = 0.6776$, Time × genotype: $F_{(4,64)} = 0.8026$, $p = 0.5280$, α-syn treatment × genotype: $F_{(1,16)} = 0.1628$, $p = 0.6919$, Time: $F_{(2.882,46.11)} = 25.40$, $^{****}p < 0.0001$, α-syn treatment: $F_{(1,16)} = 0.006116$, $p = 0.9386$, Genotype: $F_{(1,16)} = 1.846$, $p = 0.1931$, GBA1$^{+/+}$ Monomer $N = 7$, GBA1$^{+/L444P}$ Monomer $N = 6$, GBA1$^{+/+}$ fibril $N = 4$, GBA1$^{+/L444P}$ fibril $N = 4$). ***E***, Quantification of cued (three-way ANOVA: Interaction: $F_{(1,76)} = 0.03063$, $p = 0.8615$, Drug treatment × α-syn treatment: $F_{(1,76)} = 1.378$, $p = 0.2441$, Drug treatment × genotype: $F_{(1,76)} = 1.865$, $p = 0.1761$, α-syn treatment × genotype: $F_{(1,76)} = 0.6219$, $p = 0.4328$, Drug treatment: $F_{(1,76)} = 1.757$, $p = 0.1890$, α-syn treatment: $F_{(1,76)} = 5.703$, $^{*}p = 0.0194$, Genotype: $F_{(1,76)} = 1.960$, $p = 0.1656$). Control: GBA1$^{+/+}$ Monomer $N = 22$, GBA1$^{+/L444P}$ Monomer $N = 19$, GBA1$^{+/+}$ fibril $N = 9$ (one outlier removed), GBA1$^{+/L444P}$ fibril $N = 14$, Venglustat: GBA1$^{+/+}$ Monomer $N = 6$, GBA1$^{+/L444P}$ Monomer $N = 4$, GBA1$^{+/+}$ fibril $N = 4$, GBA1$^{+/L444P}$ fibril $N = 4$), and contextual fear conditioning for all mice groups. Contextual fear conditioning analysis was analyzed by evaluating the first 60 s (Interaction: $F_{(1,76)} = 0.07405$, $p = 0.7863$, Drug treatment × α-syn treatment: $F_{(1,76)} = 0.07986$, $p = 0.7783$, Drug treatment × genotype: $F_{(1,76)} = 0.3424$, $p = 0.5602$, α-syn treatment × genotype: $F_{(1,76)} = 0.2234$, $p = 0.6378$, Drug treatment: $F_{(1,76)} = 0.0002150$, $p = 0.9883$, α-syn treatment: $F_{(1,76)} = 1.850$, $p = 0.1778$, Genotype: $F_{(1,76)} = 3.979$, $^{*}p = 0.0497$), Control: GBA1$^{+/+}$ Monomer $N = 18$, GBA1$^{+/L444P}$ Monomer $N = 19$, GBA1$^{+/+}$ fibril $N = 9$ (one outlier removed), GBA1$^{+/L444P}$ fibril $N = 13$, Venglustat: GBA1$^{+/+}$ Monomer $N = 7$, GBA1$^{+/L444P}$ Monomer $N = 5$, GBA1$^{+/+}$ fibril $N = 4$, GBA1$^{+/L444P}$ fibril $N = 4$). Error bars indicate SEM. $^{*}p < 0.05$. $^{**}p < 0.01$. $^{****}p < 0.0001$.

neurons (Stoyka et al., 2020). Given how excitatory neurons show reduced expression of protein involved in degradative pathways (Fu et al., 2019), hippocampal neurons may be more vulnerable to reduced GCase activity thereby contributing to α-syn pathology. Collectively, these observations may help explain the cell-type specificity found in this study. Future studies examining GCase metabolic pathways in specific brain areas and neuronal subpopulations could reveal how mutant *GBA1* increases neuronal susceptibility in PD. However, we cannot rule out that, using the fibril model, hippocampal pathology develops at later points than in other areas, and perhaps, the reason changes are only observed in the hippocampus is because of other regions reaching a plateau in aggregate count by 10 months after injection.

Another observation that requires further observation is the opposite effect observed in motor symptoms between 3- and 12-month-old mice groups compared with the effects on contextual memory. At 3 months of age, the $GBA1^{+/L444P}$ mice exhibit a reduction in descent time in the pole test, suggesting hyperactive behavior. However, in older, fibril-injected $GBA1^{+/+}$ mice showed an increase in descent time, suggesting that development of pathologic α-syn may impair motor behavior. Future studies are needed to examine the impact of GBA1L444P expression on dopamine levels and uptake in the striatum in young and aged mice.

Previous studies showed that sphingolipids, predominantly GlcCer and GlcSph, accumulate coinciding with α-syn inclusion formation and reduced GCase activity (Mazzulli et al., 2011; Taguchi et al., 2017). However, GlcSph, but not GlcCer, accumulates in $GBA1^{+/L444P}$ mice by 6 months of age (Sardi et al., 2011; Taguchi et al., 2017). This suggests the importance of evaluating other approaches to prevent the accumulation of GlcSph specifically. Future experiments could evaluate the inhibition of acid ceramidase, an enzyme for GlcSph synthesis, or other mechanisms linked to GlcSph (Taguchi et al., 2017). The findings of GlcSph increases in the plasma in this mouse preclinical model are supported by findings that GlcSph levels are increased in the plasma of *GBA1* N370S heterozygous mutation patients compared with noncarriers (Surface et al., 2022). These findings are important because the preclinical model supports findings from human samples; thus, the $GBA1^{+/L444P}$ could be used to determine the efficacy of GlcSph as a biomarker for therapeutic efficacy in GBA1-PD.

Multiple studies demonstrated that inhibition of GCS prevents α-syn aggregate burden and GlcCer accumulation (Marshall et al., 2016; Sardi et al., 2017; Cosden et al., 2021; Viel et al., 2021). While our findings suggest that GCS inhibition alleviates aggregate burden in the mPFC, it did not prevent α-syn inclusion formation in the hippocampus or SNc of fibril-injected mice. Generally, our results did not reproduce the robust effect of GCS inhibition on synucleinopathy in vitro or in vivo. Furthermore, GCS inhibition did not rescue α-syn inclusion-induced dopamine. However, the venglustat-treated mice groups were underpowered in our study. Also, one difference between the previous studies and our study is the distinction between the GBA1L444P and D409V mutations (Johnson et al., 2021). The $GBA1^{+/L444P}$ mutation reduced GCase activity by 21.6%-31.9%, while the homozygous D409V mutation had a significantly greater reduction of GCase activity (Polinski et al., 2021). While the reduction of GCase activity may not be associated with PD risk or severity (Omer et al., 2022), it may contribute to the efficacy of GCS inhibition through other mechanisms, such as changes in CatB activity. Recently, increased expression of CatB impaired elevation of α-syn levels caused by reduced GCase activity, further supporting a potential selective role for CatB in preventing pathologic α-syn formation (Fredriksen et al., 2021). It has also been shown that pathologic α-syn itself reduces lysosome activity and prevents GCase trafficking to the lysosome (Mazzulli et al., 2011); thus, increased CatB activity may also help improve lysosome function in response to abnormal α-syn. Additionally, in $GBA1^{+/L444P}$ cultures, increases in GlcSph were not detected, unlike in $GBA1^{D409V/D409V}$ cultures (Cosden et al., 2021). Suppressing GlcCer in the absence of elevated GlcSph may therefore not be sufficient to mitigate pathology. As previously discussed, there are structural and physiological differences between hippocampal and cortical neurons, which may account for the variation in GCS inhibitor function. However, further investigation is necessary.

There are also differences in methods between these studies. For instance, variations in the generation of fibrils between laboratories is possible. Distinctions between animal models, such as transgenic expression of α-syn compared with fibril-induced corruption of endogenously expressed α-syn, heterozygosity versus homozygosity of mutations, and mouse strain background may contribute to the variations seen between phenotypes (Sardi et al., 2017; Cosden et al., 2021; Viel et al., 2021). Homozygous *GBA1* mutations model Gaucher's disease. Thus, modeling GBA1-PD more specifically is necessary for understanding the contribution of dysfunctional GCase in PD. Mice expressing the PD-specific GBA1E326K developed by Mark Cookson of the NIH (Jackson Laboratories stock #036159) may be particularly of interest. The differences between neuronopathic and non-neuronopathic mutations could be particularly important as well as the effect size of GCase activity reduction. Also, difference in the genetic background could contribute to variability across studies. For example, C57BL/6 mice perform more efficiently than a 129/Sv mouse in the Morris water maze (Hall and Roberson, 2012), yet generating a mixed background can produce a cognitive phenotype not observed in pure 129/Sv mice (Wolfer et al., 1997). In the future, comparing mice that are on the same genetic background with different *GBA1* mutations knocked in, such as neuronopathic (GBA1L444P), nonneuropathic (GBA1N370S), and non-Gaucher's/PD specific (GBA1E326K), could help dissect differences among mutations.

In conclusion, this study sheds light on the possible mechanisms by which mutant *GBA1* may increase the risk for cognitive decline by influencing pathologic α-syn formation in the hippocampus through lipid accumulation and lysosomal dysfunction as also supported by previous literature (Alcalay et al., 2010, 2012; Cilia et al., 2016; Fagan and Pihlstrøm, 2017). Further, our study highlights the potential importance of GlcSph, as a relevant biomarker for future therapeutics because of serum levels. Because GlcSph is increased in the brains of aged mice, GlcSph-targeted therapies may be effective for both GBA1-PD and idiopathic PD. Thus, this study provides a pathway for understanding how GlcSph and hippocampal pathology can impact brain function in aging and synucleinopathies as well as evaluating future therapeutic approaches to PD.

References

Alcalay RN, et al. (2010) Self-report of cognitive impairment and mini-mental state examination performance in PRKN, LRRK2, and GBA carriers with early onset Parkinson's disease. J Clin Exp Neuropsychol 32:775–779.

Alcalay RN, et al. (2012) Cognitive performance of GBA mutation carriers with early-onset PD: the CORE-PD study. Neurology 78:1434–1440.

Arrant AE, Roth JR, Boyle NR, Kashyap SN, Hoffmann MQ, Murchison CF, Ramos EM, Nana AL, Spina S, Grinberg LT, Miller BL, Seeley WW, Roberson ED (2019) Impaired β-glucocerebrosidase activity and processing in frontotemporal dementia due to progranulin mutations. Acta Neuropathol Commun 7:17.

Belmatoug N, Camou F, Serratrice C, Serratrice J, Brassier A, Rose C, Villemeur T (2017) A review of Gaucher disease pathophysiology, clinical presentation and treatments. Int J Mol Sci 18:1–30.

Bennett LL, Turcotte K (2015) Eliglustat tartrate for the treatment of adults with type 1 Gaucher disease. Drug Des Devel Ther 9:4639–4647.

Blauwendraat C, et al. (2020) Genetic modifiers of risk and age at onset in GBA associated Parkinson's disease and Lewy body dementia. Brain 143:234–248.

Boer DE, Smeden J, Bouwstra JA, Aerts JM (2020) Glucocerebrosidase: functions in and beyond the lysosome. J Clin Med 9:736.

Brunialti E, Villa A, Mekhaeil M, Mornata F, Vegeto E, Maggi A, di Monte DA, Ciana P (2021) Inhibition of microglial β-glucocerebrosidase hampers the microglia-mediated antioxidant and protective response in neurons. J Neuroinflammation 18:1–40.

Brzozowski CF, Hijaz BA, Singh V, Gcwensa NZ, Kelly K, Boyden ES, West AB, Sarkar D, Volpicelli-Daley LA (2021) Inhibition of LRRK2 kinase activity promotes anterograde axonal transport and presynaptic targeting of α-synuclein. Acta Neuropathol Commun 9:18.

Cilia R, et al. (2016) Survival and dementia in GBA-associated Parkinson's disease: the mutation matters. Ann Neurol 80:662–673.

Cosden M, Jinn S, Yao L, Gretzula CA, Kandebo M, Toolan D, Hatcher NG, Ma L, Lemaire W, Adam GC, Burlein C, Minnick C, Flick R, Watt ML, Mulhearn J, Fraley M, Drolet RE, Marcus JN, Smith SM (2021) A novel glucosylceramide synthase inhibitor attenuates alpha synuclein pathology and lysosomal dysfunction in preclinical models of synucleinopathy. Neurobiol Dis 159:1–12.

Cullen V, Sardi SP, Ng J, Xu Y, Sun Y, Tomlinson JJ, Kolodziej P, Kahn I, Saftig P, Woulfe J, Rochet J, Glicksman MA, Cheng SH, Grabowski GA, Shihabuddin LS, Schlossmacher MG (2011) Acid β-glucosidase mutants linked to Gaucher disease, Parkinson disease, and Lewy body dementia alter α-synuclein processing. Ann Neurol 69:940–953.

Do J, McKinney C, Sharma P, Sidransky E (2019) Glucocerebrosidase and its relevance to Parkinson disease. Mol Neurodegener 14:1–16.

Dopeso-Reyes IG, Sucunza D, Rico AJ, Pignataro D, Marín-Ramos D, Roda E, Rodríguez-Pérez AI, Labandeira-García JL, Lanciego JL (2018) Glucocerebrosidase expression patterns in the non-human primate brain. Brain Struct Funct 223:343–355.

Dvir H, Harel M, McCarthy AA, Toker L, Silman I, Futerman AH, Sussman JL (2003) X-ray structure of human acid-β-glucosidase, the defective enzyme in Gaucher disease. EMBO Rep 4:704–709.

Fagan ES, Pihlstrøm L (2017) Genetic risk factors for cognitive decline in Parkinson's disease: a review of the literature. Eur J Neurol 24:561–e20.

Fishbein I, Kuo YM, Giasson BI, Nussbaum RL (2014) Augmentation of phenotype in a transgenic Parkinson mouse heterozygous for a Gaucher mutation. Brain 137:3235–3247.

Fredriksen K, Aivazidis S, Sharma K, Burbidge KJ, Pitcairn C, Zunke F, Gelyana E, Mazzulli JR (2021) Pathological α-syn aggregation is mediated by glycosphingolipid chain length and the physiological state of α-syn in vivo. Proc Natl Acad Sci USA 118:e2108489118.

Froula JM, Henderson BW, Gonzalez JC, Vaden JH, Mclean JW, Wu Y, Banumurthy G, Overstreet-Wadiche L, Herskowitz JH, Volpicelli-Daley LA (2018) α-synuclein fibril-induced paradoxical structural and functional defects in hippocampal neurons. Acta Neuropathol Commun 6:13.

Froula JM, Castellana-Cruz M, Anabtawi NM, Camino JD, Chen SW, Thrasher DR, Freire J, Yazdi AA, Fleming S, Dobson CM, Kumita JR, Cremades N, Volpicelli-Daley XL (2019) Defining α-synuclein species responsible for Parkinson's disease phenotypes in mice. J Biol Chem 294:10392–10406.

Fu H, Possenti A, Freer R, Nakano Y, Villegas NC, Tang M, Cauhy PV, Lassus BA, Chen S, Fowler SL, Figueroa HY, Huey ED, Johnson GV, Vendruscolo M, Duff KE (2019) A tau homeostasis signature is linked with the cellular and regional vulnerability of excitatory neurons to tau pathology. Nat Neurosci 22:47–56.

Gomperts SN (2016) Lewy body dementias: dementia with Lewy bodies and Parkinson disease dementia. Continuum (Minneap Minn) 22:435–463.

Hall AM, Roberson ED (2012) Mouse models of Alzheimer's disease. Brain Res Bull 88:3–12.

Hamler R, Brignol N, Clark SW, Morrison S, Dungan LB, Chang HH, Khanna R, Frascella M, Valenzano KJ, Benjamin ER, Boyd RE (2017) Glucosylceramide and glucosylsphingosine quantitation by liquid chromatography-tandem mass spectrometry to enable in vivo preclinical studies of neuronopathic Gaucher disease. Anal Chem 89:8288–8295.

Henderson MX, Sedor S, McGeary I, Cornblath EJ, Peng C, Riddle DM, Li HL, Zhang B, Brown HJ, Olufemi MF, Bassett DS, Trojanowski JQ, Lee VM (2020) Glucocerebrosidase activity modulates neuronal susceptibility to pathological α-synuclein insult. Neuron 105:822–836.e7.

Hernandez AM, Silbern I, Geffers I, Tatenhorst L, Becker S, Urlaub H, Zweckstetter M, Griesinger C (2021) Low-expressing synucleinopathy mouse models based on oligomer-forming mutations and C-terminal truncation of α-synuclein. Front Neurosci 15:1–17.

Irwin DJ, White MT, Toledo JB, Xie SX, Robinson JL, Van Deerlin V, Lee VM, Leverenz JB, Montine TJ, Duda JE, Hurtig HI, Trojanowski JQ (2012) Neuropathologic substrates of Parkinson disease dementia. Ann Neurol 72:587–598.

Johnson ME, Bergkvist L, Stetzik L, Steiner JA, Meyerdirk L, Schulz E, Wolfrum E, Luk KC, Wesson DW, Krainc D, Brundin P (2021) Heterozygous GBA D409V and ATP13a2 mutations do not exacerbate pathological α-synuclein spread in the prodromal preformed fibrils model in young mice. Neurobiol Dis 159:1–11.

Leocadi M, Canu E, Donzuso G, Stojkovic T, Basaia S, Kresojević N, Stankovic I, Sarasso E, Piramide N, Tomic A, Markovic V, Petrovic I, Stefanova E, Kostic VS, Filippi M, Agosta F (2022) Longitudinal clinical, cognitive, and neuroanatomical changes over 5 years in GBA-positive Parkinson's disease patients. J Neurol 269:1485–1500.

Liu Y, Suzuki K, Reed J, Grinberg A, Westphal H, Hoffmann A, Doring T, Sandhoff K, Proia RL (1998) Mice with type 2 and 3 Gaucher disease point mutations generated by a single insertion mutagenesis procedure (SIMP). Proc Natl Acad Sci USA 95:2503–2508.

Luk KC, Kehm V, Carroll J, Zhang B, O'Brien P, Trojanowski JQ, Lee VM (2012) Pathological α-synuclein transmission initiates Parkinson-like neurodegeneration in nontransgenic mice. Science 338:949–953.

Luna E, Decker SC, Riddle DM, Caputo A, Zhang B, Cole T, Caswell C, Xie SX, Lee VMY, Luk KC (2018) Differential α-synuclein expression contributes to selective vulnerability of hippocampal neuron subpopulations to fibril-induced toxicity. Acta Neuropathol 135:855–875.

Marshall J, Sun Y, Bangari DS, Budman E, Park H, Nietupski JB, Allaire A, Cromwell MA, Wang B, Grabowski GA, Leonard JP, Cheng SH (2016) CNS-accessible inhibitor of glucosylceramide synthase for substrate reduction therapy of neuronopathic Gaucher disease. Mol Ther 24:1019–1029.

Marwaha R, Sharma M (2017) DQ-Red BSA trafficking assay in cultured cells to assess cargo delivery to lysosomes. Bio Protoc 7:e2571.

Mazzulli JR, Xu YH, Sun Y, Knight AL, McLean PJ, Caldwell GA, Sidransky E, Grabowski GA, Krainc D (2011) Gaucher disease glucocerebrosidase and α-synuclein form a bidirectional pathogenic loop in synucleinopathies. Cell 146:37–52.

Migdalska-Richards A, Schapira AH (2016) The relationship between glucocerebrosidase mutations and Parkinson disease. J Neurochem 139:77–90.

Migdalska-Richards A, Wegrzynowicz M, Id IF, Verona G, Bellotti V, Spillantini MG, Id AH (2020) L444P Gba1 mutation increases formation and spread of α-synuclein deposits in mice injected with mouse α-synuclein pre-formed fibrils. PLoS One 15:e0238075.

Mizukami H, Mi Y, Wada R, Kono M, Yamashita T, Liu Y, Werth N, Sandhoff R, Sandhoff K, Proia RL (2002) Systemic inflammation in glucocerebrosidase-deficient mice with minimal glucosylceramide storage. J Clin Invest 109:1215–1221.

Murphy DD, Rueter SM, Trojanowski JQ, Lee VM (2000) Synucleins are developmentally expressed, and α-synuclein regulates the size of the presynaptic vesicular pool in primary hippocampal neurons. J Neurosci 20:3214–3220.

Murugesan V, Chuang WL, Liu J, Lischuk A, Kacena K, Lin H, Pastores GM, Yang R, Keutzer J, Zhang K, Mistry PK (2016) Glucosylsphingosine is a key biomarker of Gaucher disease. Am J Hematol 91:1082–1089.

Mus L, Siani F, Giuliano C, Ghezzi C, Cerri S, Blandini F (2019) Development and biochemical characterization of a mouse model of Parkinson's disease bearing defective glucocerebrosidase activity. Neurobiol Dis 124:289–296.

O'Shea A, Cohen RA, Porges EC, Nissim NR, Woods AJ (2016) Cognitive aging and the hippocampus in older adults. Front Aging Neurosci 8:1–8.

Omer N, Giladi N, Gurevich T, Bar-Shira A, Gana-Weisz M, Glinka T, Goldstein O, Kestenbaum M, Cedarbaum JM, Mabrouk OS, Fraser KB, Shirvan JC, Orr-Urtreger A, Mirelman A, Thaler A (2022) Glucocerebrosidase activity is not associated with Parkinson's disease risk or severity. Mov Disord 37:190–195.

Polinski NK, Martinez TN, Gorodinsky A, Gareus R, Sasner M, Herberth M, Switzer R, Ahmad SO, Cosden M, Kandebo M, Drolet RE, Buckett PD, Shan W, Chen Y, Pellegrino LJ, Ellsworth GD, Dungan LB, Hirst WD, Clark SW, Dave KD (2021) Decreased glucocerebrosidase activity and substrate accumulation of glycosphingolipids in a novel GBA1 D409V knock-in mouse model. PLoS One 16:e0252325.

Rocha EM, Smith GA, Park E, Cao H, Graham AR, Brown E, McLean JR, Hayes MA, Beagan J, Izen SC, Perez-Torres E, Hallett PJ, Isacson O (2015) Sustained systemic glucocerebrosidase inhibition induces brain α-synuclein aggregation, microglia and complement C1q activation in mice. Antioxid Redox Signal 23:550–564.

Rocha EM, De Miranda BR, Castro S, Drolet R, Hatcher NG, Yao L, Smith SM, Keeney MT, Di Maio R, Kofler J, Hastings TG, Greenamyre JT (2020) LRRK2 inhibition prevents endolysosomal deficits seen in human Parkinson's disease. Neurobiol Dis 134:104626.

Sardi SP, Clarke J, Kinnecom C, Tamsett TJ, Li L, Stanek LM, Passini MA, Grabowski GA, Schlossmacher MG, Sidman RL, Cheng SH, Shihabuddin LS (2011) CNS expression of glucocerebrosidase corrects α-synuclein pathology and memory in a mouse model of Gaucher-related synucleinopathy. Proc Natl Acad Sci USA 108:12101–12106.

Sardi SP, Viel C, Clarke J, Treleaven CM, Richards AM, Park H, Olszewski MA, Dodge JC, Marshall J, Makino E, Wang B, Sidman RL, Cheng SH, Shihabuddin LS (2017) Glucosylceramide synthase inhibition alleviates aberrations in synucleinopathy models. Proc Natl Acad Sci USA 114:2699–2704.

Shayman JA (2010) Eliglustat tartrate: glucosylceramide synthase inhibitor treatment of type 1 Gaucher disease. Drugs Future 35:613–620.

Sidransky E, et al. (2009) Multicenter analysis of glucocerebrosidase mutations in Parkinson's disease. N Engl J Med 361:1651–1661.

Stojkovska I, Krainc D, Mazzulli JR (2018) Molecular mechanisms of α-synuclein and GBA1 in Parkinson's disease. Cell Tissue Res 373:51–60.

Stoker TB, Greenland JC (2018) Parkinson's disease: pathogenesis and clinical aspects. Brisbane: Codon.

Stoyka LE, Arrant AE, Thrasher DR, Russell DL, Freire J, Mahoney CL, Narayanan A, Dib AG, Standaert DG, Volpicelli-Daley LA (2020) Behavioral defects associated with amygdala and cortical dysfunction in mice with seeded α-synuclein inclusions. Neurobiol Dis 134:104708.

Stoyka LE, Mahoney CL, Thrasher DR, Russell DL, Cook AK, Harris AT, Narayanan A, Janado TP, Standaert DG, Roberson ED, Volpicelli-Daley LA (2021) Templated α-synuclein inclusion formation is independent of endogenous tau. eNeuro 8:ENEURO.0458-20.2021.

Surface M, Balwani M, Waters C, Haimovich A, Gan-Or Z, Marder KS, Hsieh T, Song L, Padmanabhan S, Hsieh F, Merchant KM, Alcalay RN (2022) Plasma glucosylsphingosine in GBA1 mutation carriers with and without Parkinson's disease. Mov Disord 37:416–421.

Szwedo AA, Dalen I, Pedersen KF, Camacho M, Bäckström D, Forsgren L, Tzoulis C, Winder-Rhodes S, Hudson G, Liu G, Scherzer CR, Lawson RA, Yarnall AJ, Williams-Gray CH, Macleod AD, Counsell CE, Tysnes OB, Alves G, Maple-Grødem J, Parkinson's Incidence Cohorts Collaboration (2022) GBA and APOE impact cognitive decline in Parkinson's disease: a 10-year population-based study. Mov Disord 37:1016–1027.

Taguchi K, Watanabe Y, Tsujimura A, Tanaka M (2016) Brain region-dependent differential expression of alphα-synuclein. J Comp Neurol 524:1236–1258.

Taguchi Y, Liu J, Ruan J, Pacheco J, Zhang X, Abbasi J, Keutzer J, Mistry PK, Chandra SS (2017) Glucosylsphingosine promotes α-synuclein pathology in mutant GBA-associated Parkinson's disease. J Neurosci 37:9617–9631.

Vieira SR, Schapira A (2022) Glucocerebrosidase mutations and Parkinson disease. J Neural Transm 129:1105–1117.

Viel C, Clarke J, Kayatekin C, Richards AM, Chiang MS, Park H, Wang B, Shihabuddin LS, Sardi SP (2021) Preclinical pharmacology of glucosylceramide synthase inhibitor venglustat in a GBA-related synucleinopathy model. Sci Rep 11:20945.

Volpicelli-Daley LA, Luk KC, Patel TP, Tanik SA, Riddle DM, Stieber A, Meaney DF, Trojanowski JQ, Lee VM (2011) Exogenous α-synuclein fibrils induce Lewy body pathology leading to synaptic dysfunction and neuron death. Neuron 72:57–71.

Volpicelli-Daley LA, Luk KC, Lee VM (2014) Addition of exogenous α-synuclein preformed fibrils to primary neuronal cultures to seed recruitment of endogenous α-synuclein to Lewy body and Lewy neurite-like aggregates. Nat Protoc 9:2135–2146.

Williams GP, Schonhoff AM, Jurkuvenaite A, Gallups NJ, Standaert DG, Harms AS (2021) CD4 T cells mediate brain inflammation and neurodegeneration in a mouse model of Parkinson's disease. Brain 144:2047–2059.

Wojcik SM, Rhee JS, Herzog E, Sigler A, Jahn R, Takamori S, Brose N, Rosenmund C (2004) An essential role for vesicular glutamate transporter 1 (VGLUT1) in postnatal development and control of quantal size. Proc Natl Acad Sci USA 101:7158–7163.

Wolfer DP, Müller U, Stagliar M, Lipp HP (1997) Assessing the effects of the 129rSv genetic background on swimming navigation learning in transgenic mutants: a study using mice with a modified β-amyloid precursor protein gene. Brain Res 771:1–13.

Zokaei N, McNeill A, Proukakis C, Beavan M, Jarman P, Korlipara P, Hughes D, Mehta A, Hu MT, Schapira AH, Husain M (2014) Visual short-term memory deficits associated with GBA mutation and Parkinson's disease. Brain 137:2303–2311.